Growth Twins and Deformation Twins in Metals

Irene J. Beyerlein,[1] Xinghang Zhang,[2,3] and Amit Misra[1]

[1]Los Alamos National Laboratory, Los Alamos, New Mexico 87545; email: irene@lanl.gov
[2]Department of Mechanical Engineering and [3]Department of Materials Science and Engineering, Texas A&M University, College Station, Texas 77843

Keywords

Abstract

This article reviews recent basic research on two classes of twins: growth twins and deformation twins. We focus primarily on studies that aim to understand, via experiments, modeling, or both, the causes and effects of twinning at a fundamental level. We anticipate that, by providing a broad perspective on the latest advances in twinning, this review will help set the stage for designing new metallic materials with unprecedented combinations of mechanical and physical properties.

1. INTRODUCTION AND BACKGROUND

Texture: distribution of crystallographic orientations in a material

Interest in understanding twins in metals—their origins and effects on material behavior—continues to grow. In this article, we review recent research on two categories of twins: growth twins and deformation twins. Growth twins are a result of far-from-equilibrium processing, whereas deformation twins form to accommodate strains that develop during plastic deformation. Both growth twins and deformation twins affect the properties of metals by reorienting the crystal lattice and introducing a boundary. **Figure 1a** shows an orientation map of a deformed polycrystalline metal Zr (1), in which numerous twins can be recognized by differently colored lamellae. These reoriented twin domains alter material texture and can respond to applied forces differently from those of the untwinned orientation. **Figure 1b** shows another orientation map where the reoriented (*red*) twins are favorably oriented for secondary (*blue*) twin formation (2). Because the twin and original parent lattice have different orientations, a twin boundary (TB) is introduced (**Figure 1c**). TBs can be obstacles to slip dislocations, giving rise to macroscopic hardening and strength.

Twin development involves three basic processes: nucleation, propagation, and thickening (**Figure 2**). Nucleation refers to the formation of an embryo, a volume of material within which the crystal lattice converts to twin orientation (**Figure 2a**). Upon reaching a critical size, the nucleus expands, both laterally and transversely. Lateral expansion involves the movement of a twin front (propagation, **Figure 2b**), and transverse expansion entails the migration of a TB (thickening, **Figure 2c**). The specific mechanisms underlying each stage in twin development can depend on crystal structure [e.g., face-centered cubic (FCC), body-centered cubic (BCC), and hexagonal close packed (HCP)]. Understanding and identifying these mechanisms remain an intense area of research.

This review summarizes the progress made primarily in the past decade in developing a mechanistic understanding of growth and deformation twins and places it in the context of what was learned earlier. We focus on growth twins in FCC metals and deformation twins in three common crystal structures: FCC, BCC, and HCP. The basics of twinning are not covered. For the fundamentals as well as details of earlier research, we refer the reader to existing review articles on twinning. The classical 1995 review article by Christian & Mahajan (3) provides comprehensive coverage of deformation twinning. Twinning in HCP metals is featured in reviews by Partridge (4)
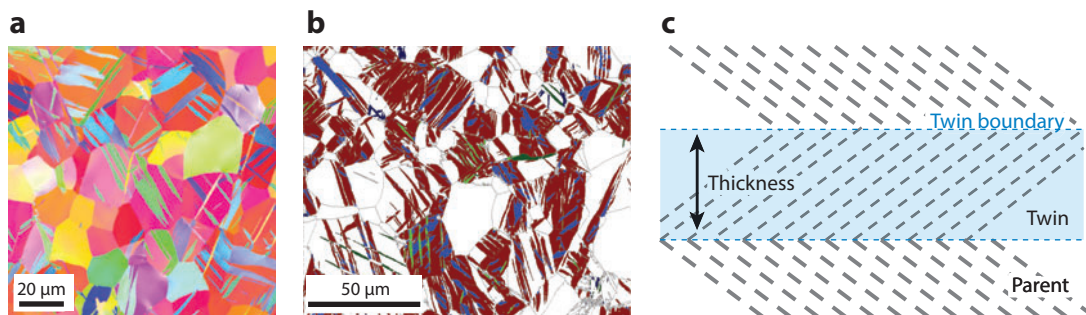

Figure 1

(*a,b*) Electron backscatter diffraction (EBSD) maps of twinned polycrystalline microstructures in deformed Zr at liquid nitrogen temperatures: (*a*) Zr (1) and (*b*) secondary (*blue*) twins within primary (*red*) twins (2). The different colors represent different crystallographic orientations. The formation of blue twins, which was not favorable in the original grain, becomes favorable within the red twinned region. (*c*) Illustration of a twin band with mirror symmetry across the twin boundary. Panels *a* and *b* adapted with permission from References 1 and 2, respectively.
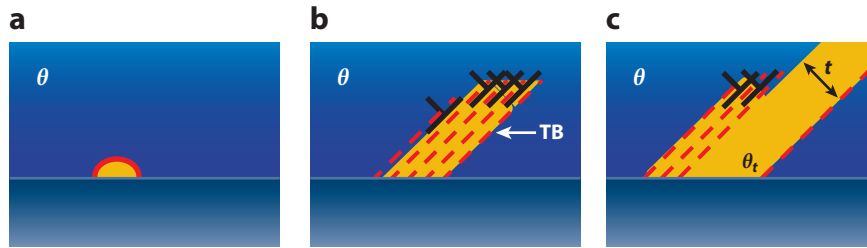
Figure 2

Illustration of the (*a*) nucleation, (*b*) propagation, and (*c*) thickening of a twin (*yellow regions*). The twin thickness (*t*) is the spacing between two adjacent twin boundaries (TBs). The bottom blue region is one grain, and the top blue region is another grain of a different crystallographic orientation. θ corresponds to the orientation of the parent grain, and θ_t is the orientation of the twin. The red dashed lines are the glide planes. The black, upside-down Ts are twinning dislocations.

and Yoo et al. (5). Zhu et al. (6) provide a recent review on deformation twinning in nanocrystalline (NC) FCC metals. Mahajan (7) recently critically reviewed models for deformation, annealing, and growth twins in FCC metals. We do not cover other twinning topics deserving of dedicated, stand-alone reviews. Such topics include twinning-induced plasticity in steels (8); annealing (5, 9), martensitic (10), or phase transformation–induced twins (11); and twinning in other low-symmetry metals, such as monoclinic, orthorhombic, or body-centered tetragonal metals (12, 13).

2. NANOTWINNED METALS WITH GROWTH TWINS

An important breakthrough in the area of twinning in metals is the fabrication of ultrastrong FCC metals with nanotwinned (NT) structures made by electrodeposition (14–16) and physical vapor deposition, such as magnetron sputtering (17–20). Nanotwins have also been observed in nanopillars and nanowires (21). These as-grown NT structures exhibit unusual and outstanding properties compared with their untwinned NC counterparts. In NC metals with high-angle grain boundaries (GBs), the increased strength typically is accompanied by losses in ductility, thermal stability, and electrical conductivity. In a remarkable contrast, NT metals, such as austenitic stainless steels, Cu, or Ag have been shown to exhibit very high strengths along with good ductility, thermal stability, and electrical conductivity at room temperature (14–20, 22).

2.1. Fabrication and Microstructure

Twin nucleation and propagation in FCC metals relies on the formation and motion of {111}<112> partial dislocations, whereas slip involves full {111}<110> dislocations. The twin planes are {111} close-packed planes, and the twinning direction is <112>. The glide of a {111}<112> partial creates a fault in the FCC stacking sequence. The energy per unit area of this fault is called the intrinsic stacking fault energy (γ_I). Growth twins are typically formed in FCC metals of low γ_I, such as austenitic stainless steels ($\gamma_I = 20$–50 mJ m^{-2}), Cu (45 mJ m^{-2}), Au (32 mJ m^{-2}), or Ag (16 mJ m^{-2}). During physical vapor deposition, {111} close-packed planes are laid down preferentially parallel to the substrate, and a higher deposition rate introduces a higher density of growth twins or stacking faults (SFs). The resulting thin film microstructures are generally comprised of GBs, coherent twin boundaries (CTBs), and incoherent twin boundaries (ITBs). GBs divide relatively large (nanometer to submicrometer)-diameter grains, which are finely laminated with nanotwins (**Figure 3a,b**) comprised of TBs that are predominantly {111}
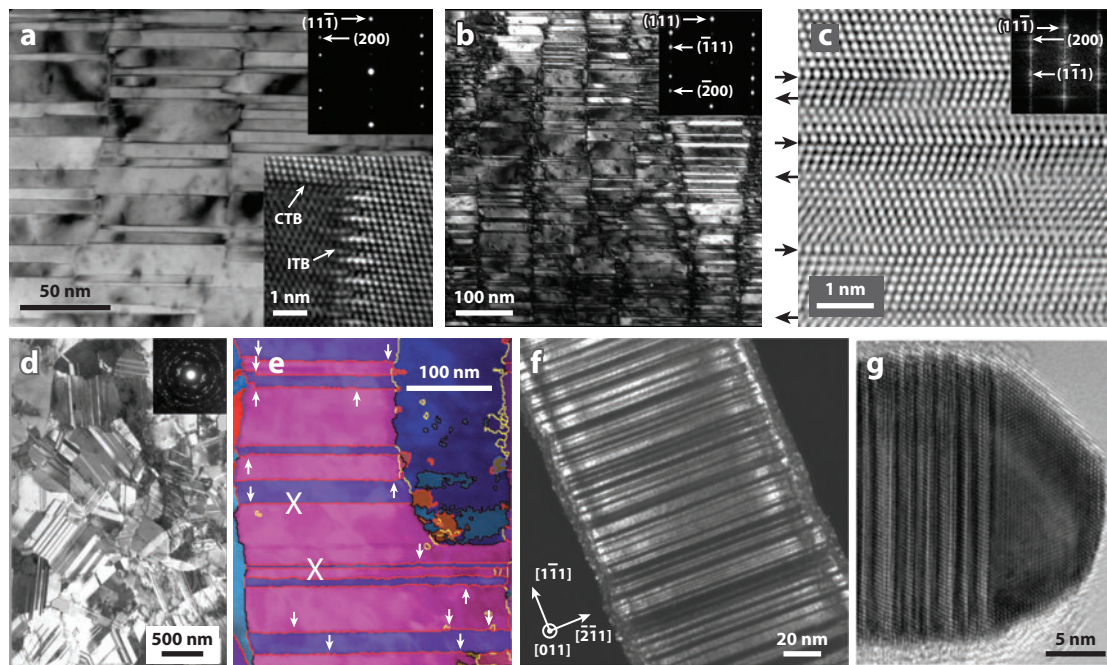
Figure 3

Bright-field transmission electron microscopy (TEM) images of magnetron sputtered (*a*) epitaxial nanotwinned (NT) Cu (23), (*b*) epitaxial NT Ag (20), (*c*) polycrystalline NT 330 stainless steel films (18) (*arrows* indicate the location of twin boundaries), and (*d*) electrodeposited (ED) NT Cu (14). (*e*) EBSD image of a defective twin boundary in sputtered NT Cu (24) (X indicates a twin boundary that has no defects, and the *white arrows* point at so-called defective twin boundaries with kinks). (*f*) Extremely fine twins in ED NT Cu nanopillars (25). (*g*) NT Au nanowires (26). Abbreviations: CTB, coherent twin boundary; ITB; incoherent twin boundary. Figure adapted with permission from References 14, 20, and 23–26.

CTBs (**Figure 3c**). The vertical front (normal to the CTB) of a nanotwin forms an ITB with the matrix and is exposed, for instance, when a NT lamella does not connect its two neighboring GBs (**Figure 3a**). Various NT metals with CTB spacing as small as several nanometers have been synthesized in columnar microstructures (epitaxial), such as Cu (23) and Ag (20) (**Figure 3a,b**), or polycrystalline microstructures, such as in NT 330 stainless steel (18) and Cu (24) (**Figure 3c,d**), and NT Cu and Au nanowires (24–26) (**Figure 3e–g**).

2.2. Hardening and Strengthening Due to Nanoscale Growth Twins

NT metals have garnered much attention following the finding that they achieve maximum hardness and strengths much higher than those of their bulk counterparts (19). For instance, the hardness and tensile strengths of NT Cu can reach 3 GPa and 900 MPa (22), compared to 500 MPa and 200 MPa, respectively, for bulk Cu. Hardness values in NC Cu and ultrafine-grained Cu (grain sizes above 100 nm) are also lower, ranging from ∼1.75 to 2.5 GPa (27, 28). These extraordinary properties are a consequence of the interactions of dislocations with the CTBs. The nanoscale spacing t between adjacent CTBs limits dislocation motion within the twin lamellae and the formation of dislocation pileups. To carry plastic deformation, dislocations must transmit across the TBs and without the aid of stress concentrations that would be associated with pileups at a boundary. Because of the large geometric misorientation angle between the {111}<110> slip
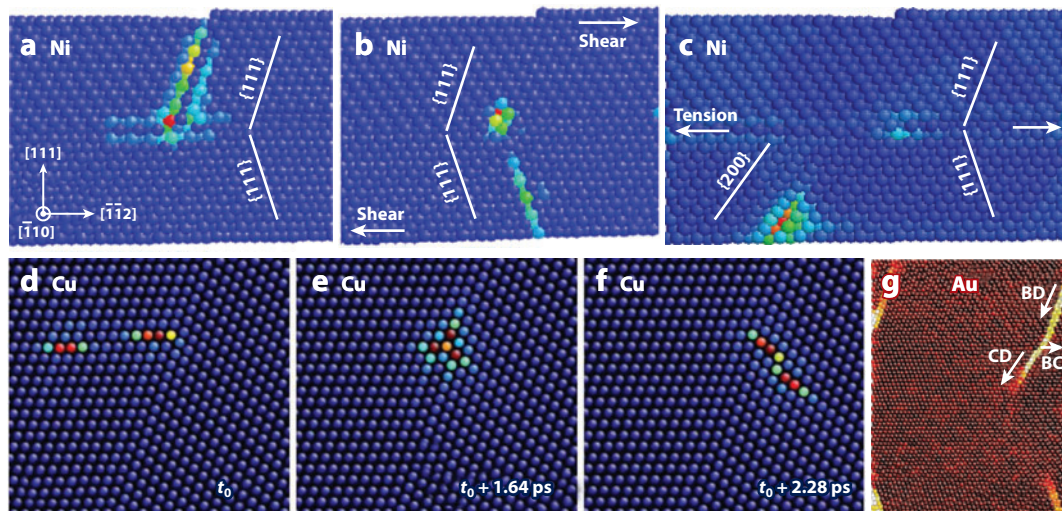
Figure 4

(*a–c*) Molecular dynamics (MD) simulations showing the interaction of a glide dislocation with a CTB in Ni. (*a*) A glide dislocation impinging on TB can either (*b*) transmit through the TB and glide onto a complementary {111} plane under applied pure shear (18) or (*c*) transmit onto an atypical {200} glide plane under tension (30). (*d–f*) A screw dislocation that encounters a TB in Cu can transmit through the TB and dissociate under shear stress (29). Panels *d–f* show snapshots with increasing simulation time, where t_0 represents the initial time. (*g*) MD simulation of dislocation transmission across a TB in NT Au (31). The color in panels *a–f* indicates the excess free energy of the atoms: Red indicates the highest free energy, followed by yellow, green, and blue. Dislocations (BC, BD, CD) are labeled using the standard Thompson tetrahedron nomenclature. Adapted with permission from References 18 and 29–31.

systems on either side of a CTB, the barrier to transmission of a single glide dislocation across a CTB is very high. Dislocation transmission across a CTB entails a sequence of events starting with the absorption of a dislocation into the TB from one side and a subsequent dissociation of the dislocation within the TB into a dislocation that can be emitted into the other side.

The details of the transmission process have been studied using molecular dynamics (MD) simulations. This process, as well as the critical transmission stress required for accomplishing the steps, generally depends on the Burgers vector, the character and sign of the impinging dislocation, and the direction of the applied stress. In a simulation of NT Ni (**Figure 4***a*), under an applied shear, a resolved shear stress on the incoming dislocation slip system of 1.7 GPa (**Figure 4***b*) is required to transmit a dislocation on a {111} plane on one side of the TB onto a complementary {111} glide plane on the other side (18). In contrast, under applied tension (**Figure 4***c*), because there is no net force to emit a glide dislocation onto a complementary {111} plane, the dislocation transmits onto a {200} plane, an atypical glide plane in FCC metals. Consequently, the resolved shear stress (again with respect to the incoming slip system) is much higher (3 GPa) (30). A simulation for Cu with TB is shown in **Figure 4***d–f*, in which an extended screw dislocation transmits across the CTB in a three-step process (29). First, the leading partial of the screw is forced to enter the CTB under a resolved shear stress of 300 MPa (**Figure 4***d*). Second, the trailing partial catches up and combines with the leading partial to form a compact full dislocation at the CTB (**Figure 4***e*). Finally, Shockley partials are emitted into the crystal on the other side of the CTB and propagate away (**Figure 4***f*). Deng & Sansoz (31) carried out MD simulations to investigate the interaction of a full dislocation with CTBs in NT Au nanopillars (**Figure 4***g*),

finding that the impinging dislocation dissociates into two full dislocations: One glides on the twin plane, and the other transmits through.

Intriguingly, the strength of a NT metal does not necessarily increase monotonically as the average twin lamella thickness (*t*) decreases. For NT metals made by electrodeposition, the strength can reach a peak value at a critical value of *t* (15, 22), as shown, for example, in the yield strength versus $t^{-0.5}$ plot in **Figure 5a** (22). This softening behavior does not occur for NT metals fabricated by sputtering, a difference also shown in **Figure 5a** (22). In the electrodeposited NT Cu studied by Lu et al. (15), the peak strength was reached at *t* = 15 nm, decreasing as *t* increased to 96 nm or decreased to 4 nm. MD simulations of NT Cu by Li et al. (32) later suggested that the twin spacing associated with maximum strength is smaller for smaller average grain size *d*, as seen in **Figure 5b**. A few explanations have been given for the apparent softening. Lu et al. (15) postulated that this softening is caused by an increase in the density of preexisting dislocations at twin interfaces that are a source of mobile dislocations. Another explanation offered is detwinning (33): When *t* becomes very fine, detwinning occurs to reduce the energy stored in the material. Detwinning of NT Cu has been observed in in situ nanoindentation and MD simulations (33) (**Figure 5d**) and under high-pressure torsion (34) (top right-hand corner of **Figure 5c**). Alternatively, large-scale MD simulations by Wu et al. (35) suggested that softening results from a transition in the deformation mechanism at a critical twin spacing. At twin spacings larger than the critical value, cross-slip and dissociation of Lomer dislocations create dislocation locks that restrict and block dislocation motion, enhancing strength. At twin spacings below the critical size, cross-slip does not occur, and instead steps form on the TBs. These steps then migrate and serve as dislocation nucleation sites, softening the material (**Figure 5e**). The divergence between sputtered and electrodeposited NT Cu (**Figure 5a**) is believed to be related to detwinning and plastic anisotropy of highly aligned {111} fiber-textured NT Cu (36). Finite element modeling has shown that the plastic anisotropy can be significant (**Figure 5f**).

A few analytical models have been developed to predict the strengthening of NT metals with a reduction in average twin spacing *t*. The basic premise is that both the GBs and CTBs in NT metals impede the glide of lattice dislocations, and NT metal strength is determined by the resistances of these dislocations to transmit across these boundaries. In the model by Gu et al. (44), the resistances to dislocation transmission across a CTB (τ_1) and GB (τ_2) are different. These authors derived the following for the flow stress of the NT metal (45):

$$\tau = \frac{\gamma_{\mathrm{I}}}{\mu b} + \frac{1}{2}(\tau_1 + \tau_2) = \frac{\gamma_{\mathrm{I}}}{\mu b} + \frac{1}{2}\left(f_1\frac{b}{t} + f_2\frac{b}{d}\right), \qquad 1.$$

where γ_{I}, μ, and *b* are the intrinsic stacking fault energy, shear modulus, and the length of the Burgers vector of dislocation, respectively. The length scales *t* and *d* are the twin spacing and grain size, respectively, and f_1 and f_2 are geometry factors related to the ratio of these two length scales.

Figure 5

(*a*) Yield strength as a function of $t^{-0.5}$ for NT Cu (22). (*b*) MD simulation of twin spacing–dependent variation of flow stress; *d* is the average grain size (32). (*c*) Detwinning observed in sputtered NT Cu after a half turn of high-pressure torsion (34). (*d*) MD simulation of detwinning in NT Cu (33) via collective glide of partial dislocations (b_1, b_2, and b_3) in the ITB plane. Excess energy is indicated by colors (*red*, highest energy; *blue*, lowest energy). (*e*) MD simulations show transition of the deformation mechanism from dislocation glide (*t* = 18.8 nm) to propagation of partials within twins (*t* = 1.88 nm); b^T is the {111} slip plane in the twin grain (35). (*f*) Orientation-dependent variation of yield stress in ED NT Cu (36) compared with CG Cu. Solid lines show EXP measurements, and shapes mark FEM calculations. (*g*) Hardness versus $d^{-0.5}$ for NT Ag (data taken from References 37–43). Abbreviations: CG, coarse grained; ED, electrodeposition; epi, epitaxial; EXP, experiment; FEM, finite element method; poly, polycrystalline; S, sputtering. Adapted with permission from References 22 and 32–43.
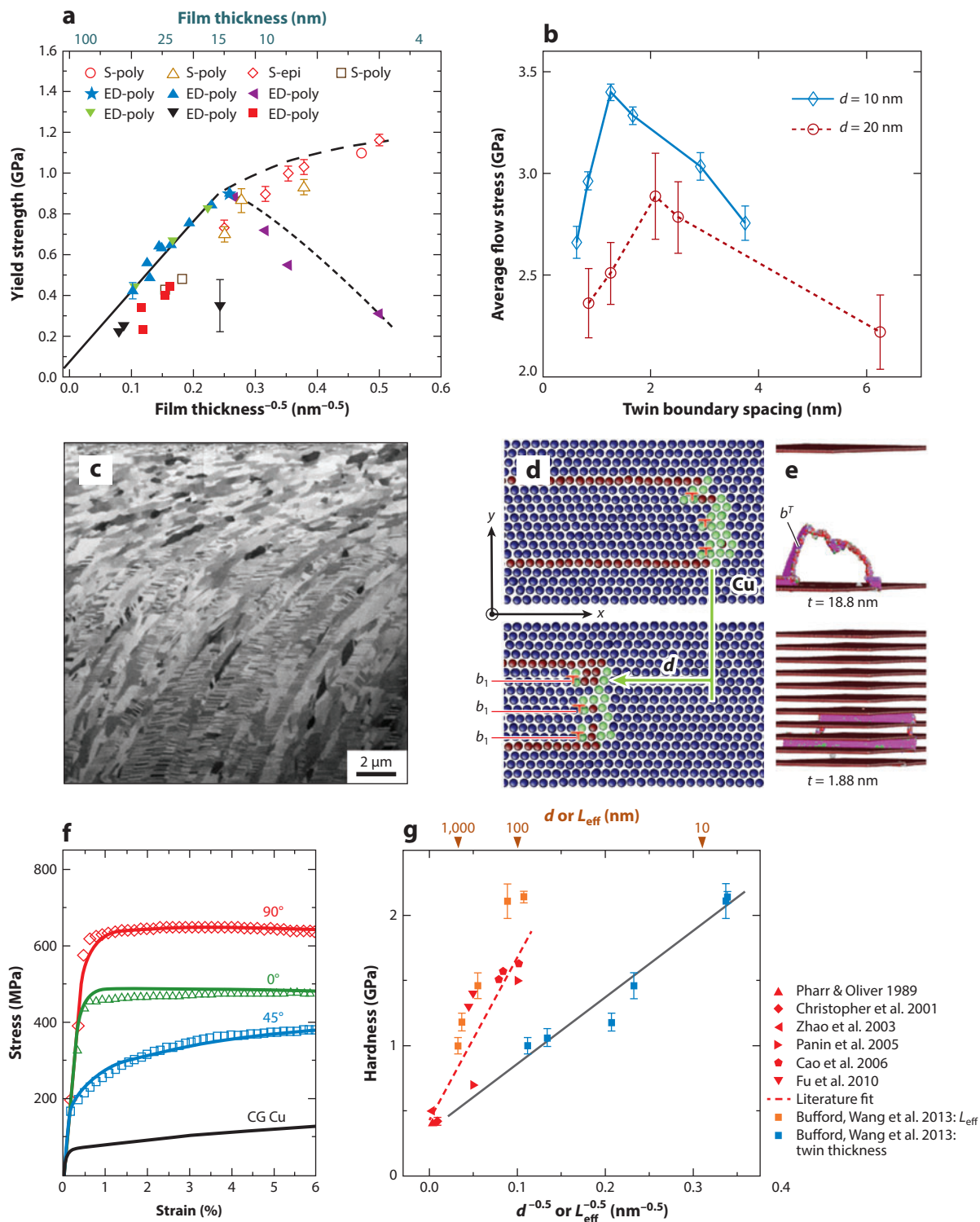
In another model by Bufford et al. (37), CTBs and high-angle GBs were assumed to have similar resistances to dislocation transmission, denoted by τ^*. In this model, the flow stress τ is given by

$$\tau = \tau_0 + \left\{ \frac{Gb\tau^*}{\pi(1-\nu)L_{eff}} \right\}^{1/2}, \qquad 2.$$

where τ_0 is the friction stress, τ^* is the flow stress for penetration of a leading partial dislocation across either the TB or GB, ν is Poisson's ratio, and L_{eff} is an effective length scale that depends on both t and d, i.e.,

$$L_{eff} = d \left[1 - \frac{t}{d} + \left(\frac{t}{d} \right)^2 \right]. \qquad 3.$$

Notice that when TBs are absent (which corresponds to $t = d$), L_{eff} reduces to d, and the traditional Hall-Petch relation is recovered. As shown in **Figure 5g**, the predictions of Equation 2 compare well with data from the literature on NT Ag. The agreement suggests that use of the average grain size d or average twin thickness t alone would not appropriately describe the size-dependent strengthening in NT metals.

2.3. Electrical Conductivity

Another extraordinary and unique property of NT metals is their apparent increase in electrical conductivity with increasing TB density. **Figure 6a** shows data from Chen et al. (45) that indicate a reduction in electrical resistivity with decreasing average twin spacing t. This behavior is not seen in coarse-grained or NC Cu, a difference attributed to the atomically ordered structure of the CTBs. Although the ordered CTBs in NT Cu and disordered high-angle GBs in NC and coarse-grained Cu alike are strong barriers to dislocation transmission, only the CTBs are weak scattering sites for electrons. A useful means of comparison is the strength-to-resistivity ratio (σ/ρ). For NT Cu, a number of studies found that a reduction in twin spacing t leads to a rapid increase in σ/ρ (**Figure 6b**) (46). However, for NC Cu, the ratio reaches a peak value with decreases in grain size d; furthermore, for equivalent characteristic length scales ($t = d$), σ/ρ is lower than that of NT Cu. Another important and related property, particularly for applications in the semiconductor industry, is stability of the microstructure against electromigration. This issue was recently studied by Chen et al. (47), who observed the migration of TBs in NT Cu under an electrical field using in situ transmission electron microscopy (TEM) (**Figure 6c**). Nevertheless, the question of resistance to electromigration deserves further exploration.

2.4. Thermal Stability

Another outstanding feature of NT metals is their thermal stability. For instance, microstructural stability up to 300°C for 3 h has been reported for NT Cu with an average t of 40 nm (28), compared to bulk Cu, which softens at 50°C. In sputtered films of {111} textured NT Cu (27) and Ag (37), the twin lamella thickness increased only moderately—from 4 to 20 nm and from 9 to 80 nm, respectively—after vacuum annealing at 800°C for 1 h (**Figure 7a,b**). At the same time, the average columnar grain size in both metals increased by an order of magnitude to more than 500 nm. Even with the combined effects of grain coarsening and minimal twin lamella coarsening, the hardness after annealing still remained high. For NT Cu, the hardness decreased gradually with annealing temperature (each held at 1 h); at the highest temperature anneal—800°C for 1 h—hardness was 2.2 GPa (**Figure 7e**).

The excellent thermal stability of NT metals arises from the high density of low-energy CTBs. For instance, in Cu, CTBs have a formation energy of 24–39 mJ m^{-2}, which is much lower than
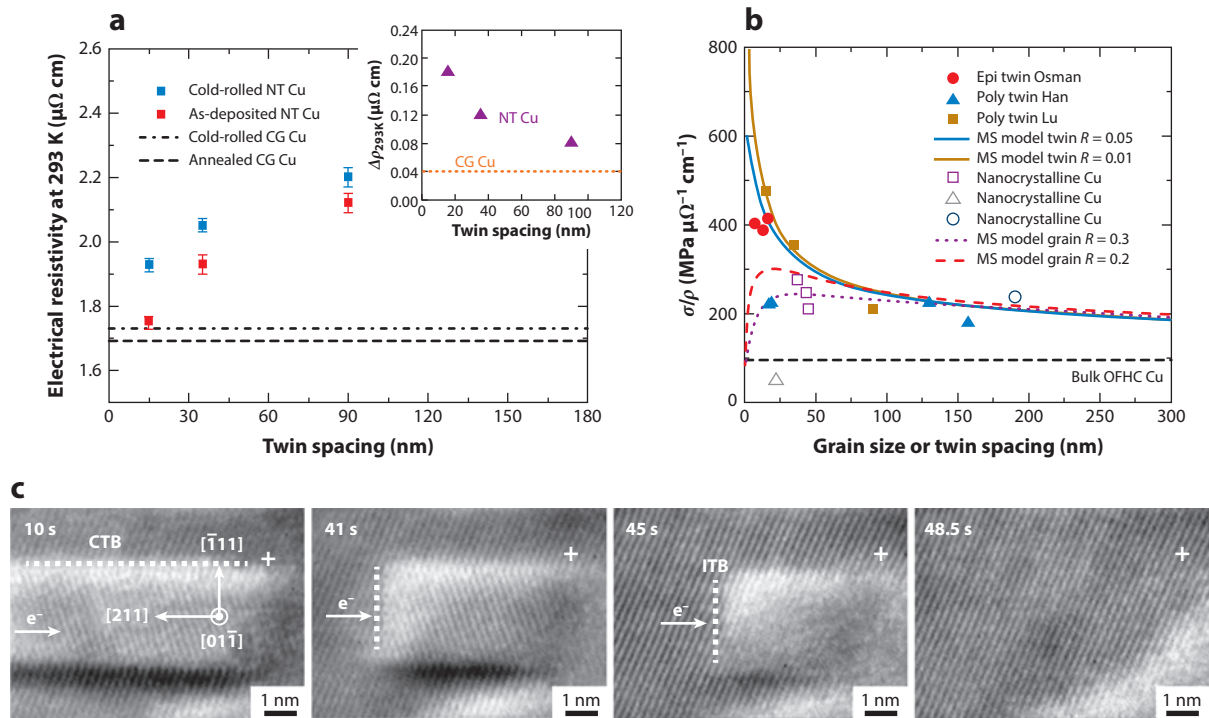
Figure 6

(*a*) Reduction of electrical resistivity with decreasing twin spacing for ED NT Cu (45). (*b*) The strength-to-resistivity ratio (σ/ρ) increases monotonically with decreasing twin spacing, whereas a maximum exists for nanocrystalline (NC) Cu (46). Data taken from References 45, 48–51, and 59. (*c*) In situ TEM images of TB migration under an electrical field (47). Abbreviations: MS, Mayadas and Shatzkes; OFHC, oxygen-free high conductivity. Adapted with permission from References 45–51.

that of ITBs (590 mJ m^{-2}) and GBs (typically 625–710 mJ m^{-2}). Thus, under thermal annealing, the driving forces for grain coarsening and removal of ITBs are much higher than for twin lamella coarsening. This difference explains why in the aforementioned study by Anderoglu et al. (27), the grains grew but the twin lamella grew only modestly. Likewise, a more recent study reported the thermal stability of NT Cu was better than that of NC Cu containing equiaxed grains of similar diameter and mostly high-angle GBs (28). Compared to {111} textured NT Cu ($t =$ 40 nm), which does not coarsen until 300°C, NC Cu ($d = $ 40 nm) coarsened rapidly at temperatures as low as 200°C (28), and its hardness began to decrease significantly after annealing at 400°C for 3 h (27) (**Figure 7*e***). Beyond 300°C, coarsening in {111} textured NT Cu is initiated by the thermally activated motion of the ITBs followed by lateral motion of the high-angle GBs of the columnar grains, again demonstrating that the CTBs are the most stable. For similar reasons, NT microstructures with a higher fraction of ITBs, such as the {110} textured NT metals (**Figure 7*c***), are not as stable as the {111} textured NT metals. This difference causes an apparently strong orientation dependence on thermal stability, which has been studied in NT Ag (37). Under heating at 800°C for 1 h, the ITBs exited the film via propagation to the free surface, resulting in twin lamella coarsening (**Figure 7*d***). On this basis, one can envision that the coarsening in NT thin films may be hindered by the introduction of impurities, which act as pinning sites. For example, NT Cu with Fe impurities is more thermally stable than high-purity NT Cu (27).
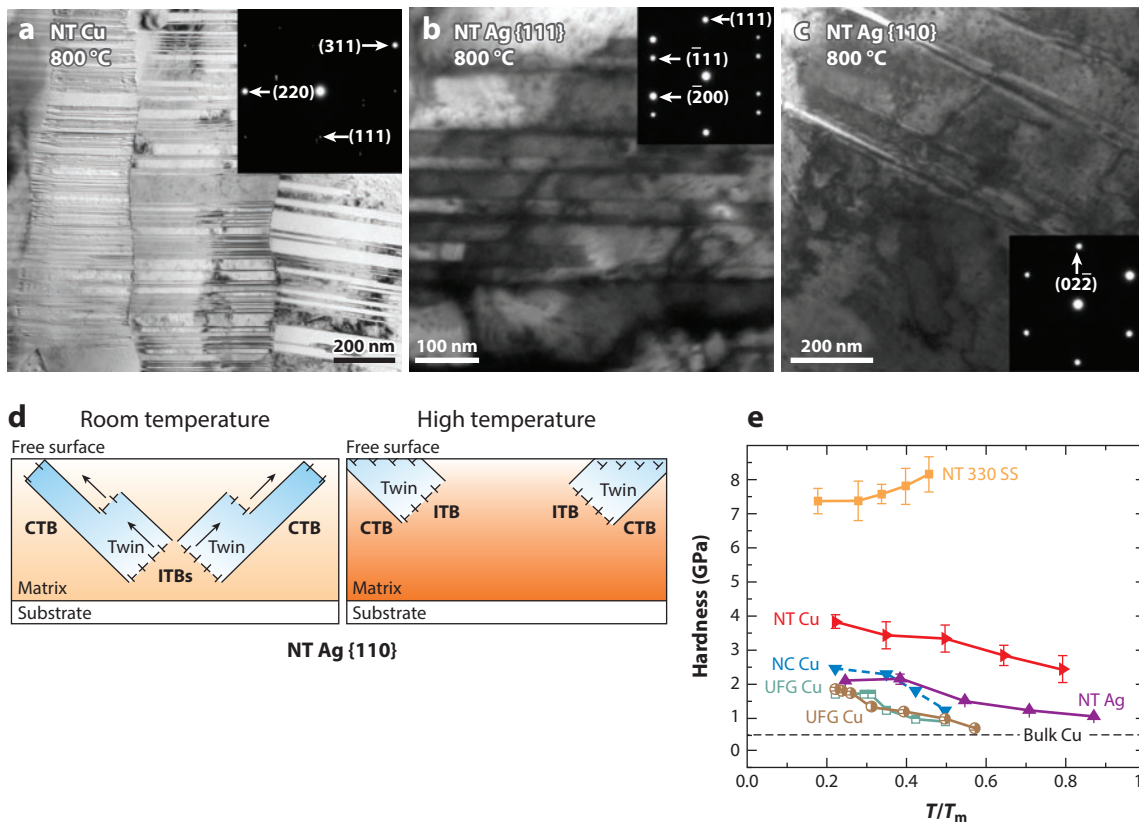
High-density nanotwins remained in sputtered (*a*) NT Cu (27) and (*b*) NT Ag (37) with {111} textures up to 800°C. (*c*) Twins were rarely seen in NT Ag {110} after annealing at 800°C. (*d*) Mobile Shockley partials preferentially migrate to the free surface in annealed NT Ag {110} (37). (*e*) The hardness of {111} textured NT Cu, Ag, and 330 stainless steel (330 SS) remained high after annealing compared to a drastic softening in NC and ultrafine-grained (UFG) Cu (27). Reprinted with permission from References 27 and 37.

2.5. Synthesis of Nanotwinned Structures in High Stacking Fault Energy Materials

Most NT metals studied to date are low-γ_I FCC metals and alloys, such as austenitic stainless steels, Ag, and Cu, which can form nanotwins readily at high deposition rates. For materials with relatively higher γ_I values, such as Ni (120–144 mJ m^{-2}), sputtering at a very high deposition rate is needed to form high CTB densities (52). Using the same method to form nanotwins in metals with even higher γ_I values, such as Al or Pd with γ_I values in the range of 140–180 mJ m^{-2}, is likely to be difficult. As an alternative, researchers have used intermediate layers of another material to form NT Al.

In one example, intervening, polarized, nanoscale ceramic layers were used. In vapor-deposited Al/TiN/Al nanolayers, when the TiN intermediate layer was less than ∼2 nm, the Al layers below and above the TiN layer grew in a twin orientation (53) (**Figure 8a**). Density functional theory (DFT) calculations (**Figure 8a'**) revealed that N termination in the {111} growth plane of the TiN layer energetically favors the growth of Al layers in a stacking sequence that is twinned with
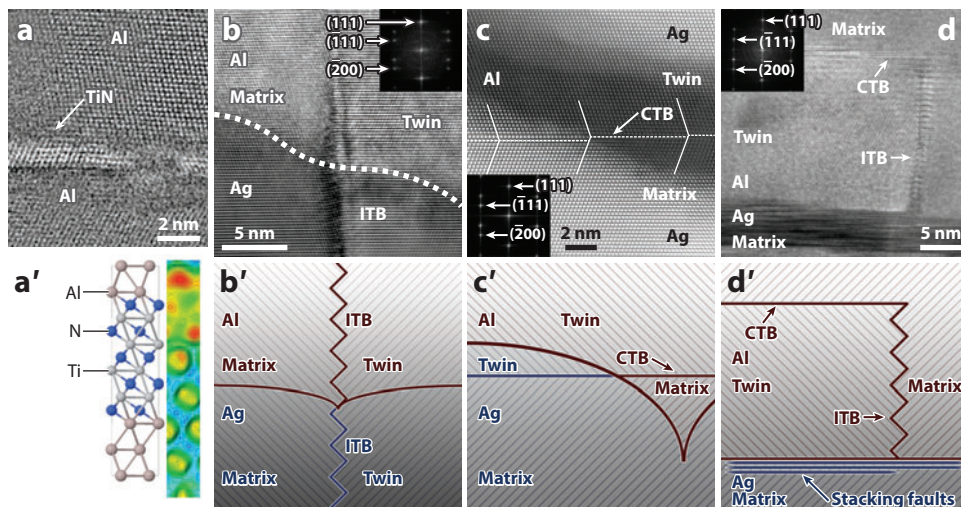
Figure 8

(*a*) Scanning transmission electron microscopy (STEM) high-resolution image of Al/TiN multilayers showing that the TiN layer has the same orientation as the Al layer below it, whereas the top Al layer has a twin orientation with respect to the underlying TiN and Al layers (53). (*a'*) The relaxed interface structure in twinned Al/TiN/Al calculated from density functional theory and the electron localization function at the same interface (53). Colors represent increasing electron density at the Al/TiN (*red*, highest density; *blue*, lowest density). (*b–d*) The formation of high-density growth twins in Al through Ag seed layers (55). Panels *b* and *d* are high-resolution transmission electron microscopy (HRTEM) micrographs, whereas panel *c* is a STEM micrograph. (*b'–d'*) Twin formation mechanisms in Al. Twins nucleated in the Ag seed layer can penetrate either vertically (*b* and *b'*) or laterally (*c* and *c'*) into Al, as Ag and Al have a very small lattice mismatch. Panels *d* and *d'* show ITBs nucleating from high-density stacking faults at the Al/Ag interface. Adapted with permission from References 53 and 55.

respect to the Al layer below (53). If the TiN layer is Ti-terminated instead of N-terminated, the energetic preference for twin stacking is lost. Furthermore, this unusual atomic stacking across metal/ceramic interfaces enables the metal layers to deform at very high stresses and the nanolayered ceramic to deform plastically (53, 54).

Another study demonstrated NT Al can be fabricated in sputtered Al/Ag multilayers, wherein the intermediate layer Ag is relatively thin (100 nm) compared to the Al layer (1,000 nm). In the Al layer of the composite, abundant growth twins—some as wide as 100 nm—and SFs were observed (55, 56). The hardness of this predominantly NT Al metal reached ~1.2 GPa, one of the highest values reported to date for Al films (55).

In this composite system, the other phase, Ag, is a metal that forms nanotwins easily. Because it has a low lattice mismatch with Al, less than 1%, it forms a nearly coherent interface with Al. These features facilitate three mechanisms for Al NT formation. In the first mechanism (**Figure 8*b*,*b'***), an ITB formed in Ag extends vertically into Al through the Al/Ag layer interface (55). Because of the nearly coherent structure of the Al/Ag interface, the orientations of the Ag domains and Ag ITBs are replicated almost exactly in the Al layer. Similarly, in the second mechanism, coherency of the Al/Ag interface facilitates lateral propagation of CTBs in Ag into Al (**Figure 8*c*,*c'***). A similar TB replication mechanism has also been observed in the Cu/Ni system, wherein CTBs that originated in the Cu layer extended into Ni (57). A third but less understood mechanism has also been proposed: ITBs may nucleate directly from the Al/Ag interface, where a high density of SFs presumably exists on the Ag side (**Figure 8*d*,*d'***).

Recently, NT structures have also been synthesized in nonmetallic materials such as HgCdTe (58) and cubic boron nitride (BN) (59). The NT cubic BN bulk samples demonstrated unprecedented mechanical and physical properties: optical transparency, hardness exceeding 100 GPa, oxidization resistance up to 1,200°C, and a fracture toughness of >12 MPa$\sqrt{m}$.

2.6. Challenges and Future Prospects in Nanotwinned Metal Research

The progress made in NT metals has inspired new directions and challenges for future research in this area. First, there is a need to synthesize bulk NT materials. Recent studies have demonstrated that nanotwins can be introduced into bulk steels (60, 61) and superalloys (62). The radiation response of NT metals is also largely unexplored. Severe radiation damage poses significant challenges to the application of metallic materials in nuclear reactors. The interaction of nanotwins with radiation-induced point defects was recently investigated in References 63 and 64. Although CTBs appear to have a low sink efficiency for point defects and He (63), ITBs seem to be effective defect sinks (64). Furthermore, the migration of both CTBs and ITBs under irradiation conditions can remove defect clusters such as SF tetrahedra (64). Because detwinning is frequently observed in NT metals, it is worthwhile to develop microstructural design strategies, e.g., through alloying, to induce solute segregation or precipitation at TBs to stabilize nanotwins under high stresses and high temperatures.

3. DEFORMATION TWINNING

The plastic deformation of a metal is accommodated primarily by the motion of slip dislocations. For some metals under certain conditions, deformation twinning can occur in addition to slip. In these metals, twinning is promoted at high strain rates (65–69), low temperatures (70, 71), or both. Twinning occurs heterogeneously throughout the material, and twins within the same material typically vary widely in thickness (72–74) (**Figure 1**). Twins usually develop at material locations characteristically high in stress concentration, defects, or both. They often occur near GBs, dislocation pileups, surface defects, slip bands, kink bands, twin interfaces, and cracks (75–81). Twins preferentially emit from GBs (e.g., **Figure 9** and Reference 78), free surfaces, and interfaces (79, 82–84).

Twins reorient the crystal lattice and impart a TB (**Figure 1**) (85). During deformation, twins can evolve in size. With straining, reoriented twin domains can lengthen or shorten, thicken or shrink, and remain separated or coalesce. These changes are associated with TB creation, migration, coalescence, and absorption into a GB. Within an evolving reoriented twin domain, new slip or twinning can take place (a volume effect). With evolving TBs, mobile slip dislocations or growing intersecting twins (a boundary effect) can be pinned or transmitted. As a result of the above effects, deformation twinning significantly alters material flow stress, work hardening, plastic anisotropy, and the dependencies of plastic response on temperature and strain rate (73, 85–89, 90–93).

Twinning is less well understood than dislocation slip. Achieving a mechanistic understanding of where, when, and how deformation twins form and evolve still remains a rich and important area of research. As we discuss below, much exciting progress has been made over the past decade, particularly on the elusive problem of twin nucleation.

3.1. Twin Nucleation

Over the years, deformation twin nucleation models have been classified as either homogeneous (94–96) or heterogeneous (72, 97–109). Heterogeneous nucleation refers to a nucleation process
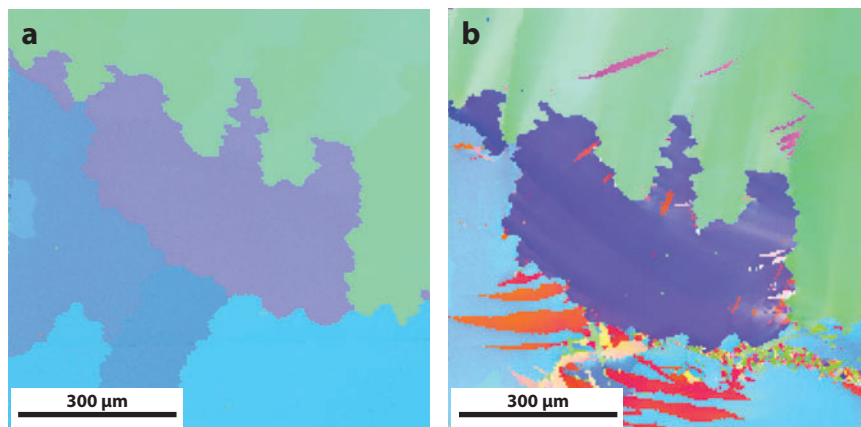
Figure 9

In situ EBSD image of an Mg-Ce alloy under deformation showing the nucleation of twins from grain boundaries at (*a*) an early stage at lower strain and (*b*) after more straining. The different colors correspond to different crystallographic orientations. Figure adapted from Reference 78.

that results from the presence of a defect, and homogeneous nucleation refers to one that does not. To date, homogeneous nucleation models have found little experimental support (3, 110). Recent approaches have used heterogeneous nucleation models. The stresses associated with heterogeneous nucleation models are lower than those required for homogeneous nucleation (110, 111). In some cases, nucleation stresses from heterogeneous nucleation models have attained reasonable agreement with indirect experimental measurement (79, 112, 113).

In most heterogeneous nucleation models, twins form from a dislocation defect. The initiating dislocation is considered to be either lattice dislocations (97, 100–108) or dislocations found in GBs (109, 112, 114) or bimetal interfaces (115, 116). Under a suitable stress and through a series of steps, the dislocation transforms into a stable twin nucleus; stable means that under the applied stress, the twin nucleus either retains its configuration or propagates as a twin into the crystal.

Although the details of the mechanisms and pathways involved in forming a stable nucleus from one or more defects may differ between models, dislocation dissociation reactions are usually involved. Before presenting various twinning models, we review some basic rules of dissociations, which provide necessary but insufficient conditions for twinning (117, 118). In the context of twinning, a dissociation reaction converts a dislocation with Burgers vector b on plane n into a product of two or more dislocations with Burgers vectors b_1, b_2, and so forth. **Figure 10** illustrates a simple dissociation reaction in which one product dislocation b_1 is a twinning dislocation (TD) on the twin plane n_T and the other is the residual dislocation b_R, e.g.,

$$b \rightarrow b_R + b_1 \qquad\qquad 4.$$

The basic rules of this reaction are: (*a*) The line of the dislocation b must coincide with the line of intersection of the slip plane n and twinning plane n_T; (*b*) the Burgers vectors must be conserved, i.e., $b - b_R + b_1 = 0$; and (*c*) the interaction forces between the TD(s) and the residual dislocation are repulsive. The dissociation reaction may directly lead to a TD (as shown) or to other defects, which are involved in nucleus formation. Regardless of the role dissociation reactions play in the proposed mechanism for twinning, these rules must be satisfied.
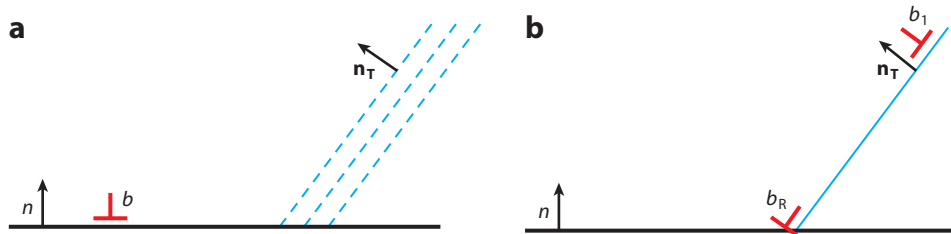
Figure 10

Illustration of a nonplanar dissociation of a dislocation with Burgers vector b (*a*) before as it glides on its plane with normal $\mathbf{n_T}$ and (*b*) after the dissociation when it produces a residual b_R and another dislocation with Burgers vector b_1 onto its plane with normal $\mathbf{n_T}$.

3.2. FCC Metals

As mentioned in Section 2.1, the elementary TD responsible for twinning in an FCC metal corresponds to a Shockley partial on the {111} plane with a Burgers vector of $(a/6)<112>$. There are 12 {111}$<112>$ twinning systems. These can be conveniently designated using the Roman/Greek nomenclature (e.g., Aδ, δB) in the Thompson tetrahedron (**Figure 11**) (3, 110).

The energies involved in the formation of these partials are related to the material γ-surface on the {111} twinning plane (6, 119–124). This is a three-dimensional (3-D) surface of the excess energy corresponding to rigid displacements of one half of a crystal relative to the other half. For FCC twinning, the relevant energy-displacement section of the γ-surface is associated with rigid displacements in the $<112>$ direction, which is called the generalized stacking fault energy
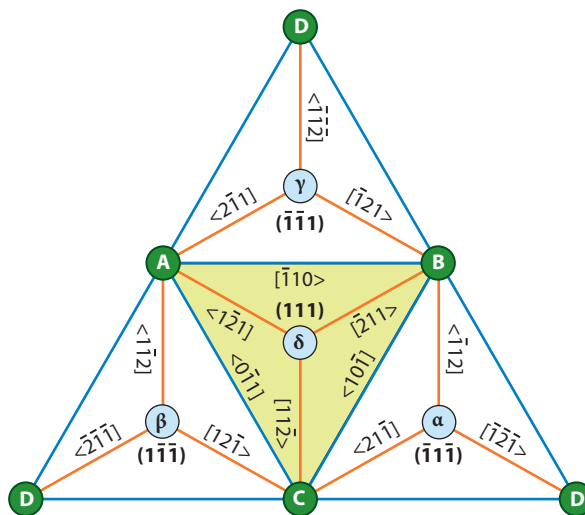

Figure 11

The unfolded Thompson tetrahedron with its four faces lying in the same plane. The four faces correspond to the four independently oriented {111} planes; the vertices A, B, C, and D (*green circles*) to lattice points; and the edges between vertices (e.g., AB, CB; *blue lines*) to the Burgers vectors of the 12 full dislocations. The Greek points (α, β, γ, δ; *light blue circles*) in the centers of the {111} planes (faces) do not correspond to lattice points, and the 12 vectors connecting a vertex to a Greek point (e.g., Aδ, δB; *orange lines*) are the Burgers vectors of the Shockley partials. See also Reference 110.
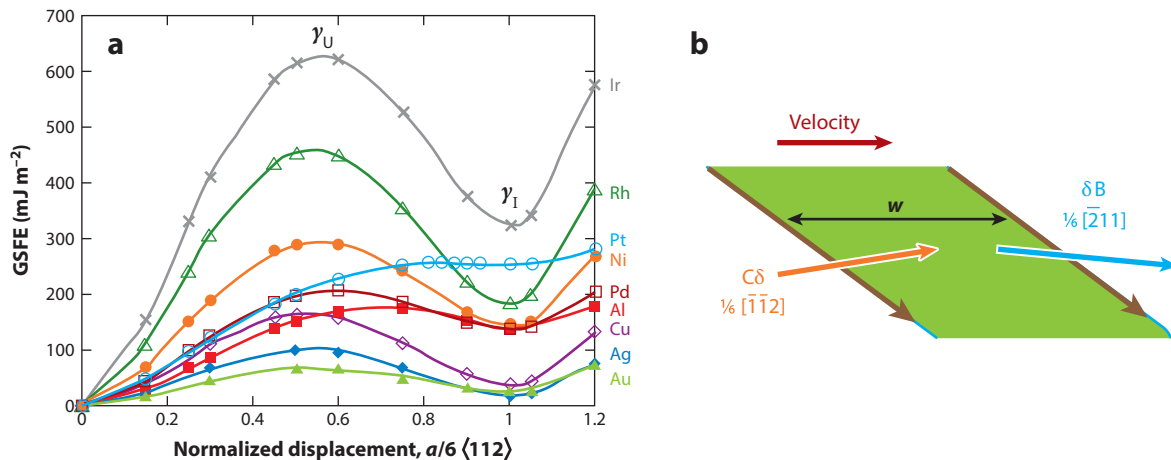
Figure 12

(*a*) Generalized stacking fault energy (GSFE) curves for various face-centered cubic (FCC) metals as calculated by density functional theory. This is a section of the 3-D γ-surface. The intrinsic stacking fault energy γ_I and the unstable stacking fault energy γ_U are marked. Panel *a* adapted from Reference 124. (*b*) Planar dissociation of a dislocation into two Shockley partials on either side of a stacking fault of finite width w.

(GSFE) curve. **Figure 12a** shows GSFE curves for several FCC metals calculated by DFT (124). The displacement produced by a single Shockley partial (e.g., Cδ or δB in **Figure 11**) corresponds to a local energy minimum with energy γ_I in the GSFE curve. Because the atomic positions associated with this minimum do not correspond to lattice points, this displacement causes the FCC stacking to become faulted.

Because a Shockley partial corresponds to an energy minimum in the γ-surface, it and the intrinsic SFs it creates can be stable in a perfect FCC crystal. This implies that slip dislocations in FCC metals are partial dislocations and that dislocation sources emit partial dislocations. FCC metals can deform by full dislocations; these dislocations are not compact but extend into two Shockley partials on either side of an intrinsic SF of width w. **Figure 12b** shows a full dislocation CB as an extended dislocation. This configuration is the result of a dissociation reaction written as CB $\rightarrow$ Cδ + δB. When the dislocation moves from C to B (in the direction shown), then δB is the leading partial and Cδ the trailing partial. From dislocation sources, full dislocations are created by sequential nucleation of the two partials: the leading (the first to nucleate) and the trailing partial.

Because the common slip dislocation of an FCC metal, a Shockley partial, can also correspond to a TD, twinning has been roughly correlated with the size of w (**Figure 12b**). The equilibrium SF width w_0 is its value under no stress and is determined by a balance of the repulsive force of the two partials and the attractive (restoring) force of the SF. With these considerations, the normalized width w_0/b varies inversely with the dimensionless parameter $\gamma_I/\mu b$ (110, 125, 126). The value of $\gamma_I/\mu b$ for Ni is 2.3 times higher than that for Cu; consequently, w_0 is approximately 2.3 times larger for Cu than for Ni. Under stress, however, w can widen or narrow with respect to w_0 (110, 125, 126). Widening ($w_d > w_0$) occurs when the applied load is oriented with respect to the crystal lattice, causing the leading partial to experience a higher resolved shear stress than the trailing partial. Sufficiently large values of stress can even overcome the restoring force, causing the dislocation to split (w_d approaches infinity). Deformation twinning in FCC metals has been

associated with grains that are crystallographically oriented such that the applied stress causes w_d to widen (66, 127). Narrowing ($w_d < w_0$) happens in the opposite situation, in which the trailing partial has a higher resolved shear stress. This case is associated with slip, not twinning. The simple narrowing/widening concept provides an explanation for some but not all cases of orientation-dependent FCC twinning (7). More sophisticated models for orientation dependence consider the mechanisms of twin nucleus formation and growth and are reviewed below.

The width w also depends on the intrinsic SF energy γ_I. As a rule of thumb, the tendency for FCC twinning increases as γ_I decreases (3, 102). This relationship arises because work must be done to separate the TD from the dissociation site and to extend the SF with an energetic penalty of γ_I. Returning to the example above, $\gamma_I/\mu b$ for Cu is lower than that for Ni, and experiments show that Cu twins more readily than Ni (6, 128). Ag, which has a very low γ_I of 16–20 mJ m^{-2} (**Figure 12a**), also requires relatively little stress to twin at room temperature (23, 77), whereas Al, which has one of the highest γ_I values (140–166 mJ m^{-2}) (**Figure 12a**), twins only at extreme conditions of high stress, such as at crack tips or in nanograins ($\sim$10 nm) (75, 129). Last, alloying an FCC metal leads to both increases in the propensity for twinning and decreases in γ_I (67, 69, 130, 131).

The above discussion simply connects twinning with the creation of an SF by a propagating TD (the Shockley partial) and creating a single fault. However, a twin domain is not a single fault but rather consists of layers of adjacent faults. In efforts to increase precision, more recent attempts have linked the propensity for twinning in FCC metals with the nucleation and thickening processes of twinning. Because a single-layer SF is stable, an FCC twin may form via the sequential nucleation and propagation of TDs on adjacent parallel {111} planes (or layers). After formation of the first layer, the glide of a second TD on a plane adjacent to this first fault creates a two-layer twin, as shown in **Figure 13a**. **Figure 13b** shows the corresponding energetic landscape, called the generalized planar fault energy (GPFE) curve, which considers both first- and second-layer formation. The energetic barrier to create the second neighboring TD is termed the unstable twin fault energy (γ_{UT}). The energy of the two-layer fault is called twin fault energy (γ_T). Thickening or boundary migration of the twin can continue via glide on the third layer, the fourth layer, and so on.

Based on this twin formation mechanism, more refined twinnability measures have been developed that include other fault energies beyond γ_I from the GPFE curves. These include measures suggesting that twinning is associated with low ratios $\Delta = \gamma_I/\gamma_U$ (121, 123), high difference $\gamma_{UT} - \gamma_U$ (132), or high $T = (1.136 - 0.151\gamma_I/\gamma_U)\sqrt{\gamma_U/\gamma_{UT}}$ (122). Collectively, these measures reflect that low γ_I relative to γ_U and low γ_{UT} relative to γ_U favor twinning. For example, the ratios $\Delta = \gamma_I/\gamma_U$ for Cu and Ni are 0.235 and 0.5, respectively (**Figure 12a**), indicating Cu has a higher likelihood of twinning than Ni; as mentioned above, this is in agreement with experimental data. These twinnability measures have proven useful for providing ranked propensities for twinning among FCC metals and their alloys. They do, however, require that reliable estimates for stacking energies and GPFE curves are known.

An important question for twin nucleation concerns the minimum number of layers required for a stable FCC twin nucleus. Atomistic simulations, such as DFT and MD, have employed an energy-based method for determining stable nuclei sizes. These calculations assume, as we have thus far, that the pathway toward building a twin proceeds by layer-by-layer TD glide (**Figure 13b**). In this method, the excess potential energy associated with inserting each additional layer is calculated. The number of layers at which the total stacking energy converges to a steady-state value is considered the stable nucleus size. Such calculations suggest that a stable FCC twin nucleus contains two to three layers, depending on the method used and alloys added (113, 120, 123).
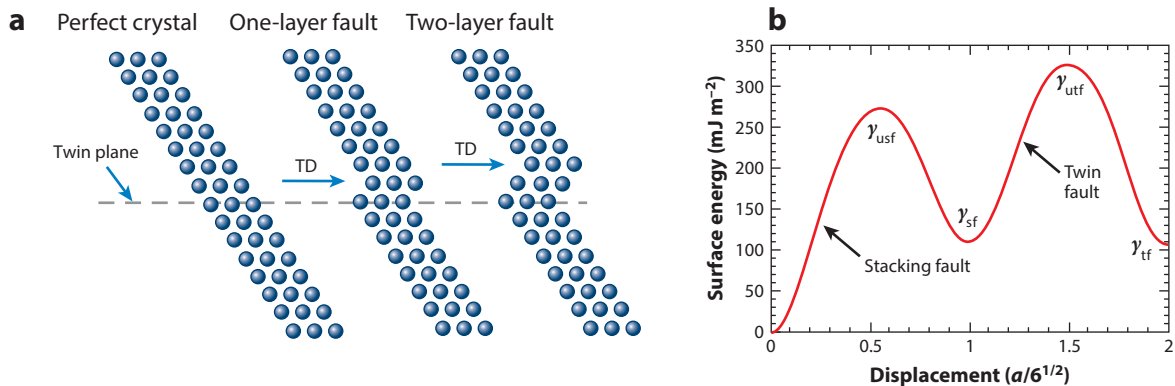
a Perfect crystal · One-layer fault · Two-layer fault

b

Figure 13

(*a*) Effect of glide of a Shockley partial on a {111} plane and formation of a two-layer twin by sequential glide of an identical partial on an adjacent {111} plane. (*b*) A typical generalized planar fault energy curve for an FCC metal. Abbreviations: TD, twinning dislocation; γ_{sf}, intrinsic stacking fault energy; γ_{tf}, twin fault energy; γ_{usf}, unstable stacking fault energy; γ_{utf}, unstable twin fault energy. Panel *b* taken from Reference 6.

Natural formation of a stable twin nucleus may not necessarily develop via layer-by-layer glide of TDs. Many mechanisms for forming the two- to three-layer nucleus have been proposed, all involving high stress and dislocation dissociations. These mechanisms include pole mechanisms (101, 102, 110), the dissociation of single dislocations (66, 102, 127), dissociation reactions of two coplanar (108) and two nonplanar (97) slip dislocations, sequential emission of TDs from GBs (133, 134), and simultaneous or synchronized emissions of groups of TDs with different Burgers vectors with a net value of zero (zero-strain twinning) (135, 136). Validating any of these mechanisms via in situ observation is challenging.

The next stage of twin development after twin nuclei formation is emission into the crystal, propagation across the grain cross section (**Figure 2*b***), and twin thickening (**Figure 2*c***). The processes of thickening the twin (or migrating the TB) may simply involve adding more layers to the twin nucleus by repeating the aforementioned nucleation events on adjacent planes. Other mechanisms for twin thickening have also been proposed. These include glide dislocations that run into a TB and dissociate into a TD that can subsequently glide on the TB, advancing it by one layer (137); nucleation of a TD dipole between two separate SFs (133); and rebound of a TD off a boundary onto the adjacent plane (110, 138, 139).

As well as satisfying the rules of dislocation dissociation (Section 3.1), some of the above nucleation and thickening mechanisms have additional constraints. For instance, the Mahajan-Chin mechanism, involving dissociation of two coplanar slip dislocations, requires coplanar slip (108); the dissociation of a single dislocation needs certain crystallographic grain orientations that widen w_d (66, 109); and the rebound mechanisms operate when dislocations move at high velocities (138).

In addition to crystal orientation and intrinsic material properties (e.g., γ-surface), grain size influences the propensity of an FCC metal to twin. Numerous experimental studies have reported that reductions in grain size hinder twinning (140). This trend, however, does not extend into the nanoscale grain-size regime, in which twinning remarkably becomes more prevalent (6). In fact, the nanoscale size effect is so strong that metals that normally do not twin as coarse-grain structures have been observed to twin as nanograin structures. Stacking faults and twins have been seen in crystals that are ∼150 nm or smaller in Cu at room temperature (70, 83, 141), ∼25 nm

Pole mechanisms: models to explain twin nucleation and growth that require a stable pole dislocation with Burgers vector normal to the twin plane (*n*) and a TD on *n* that rotates around this pole

in Ni at liquid nitrogen temperatures (6, 142), ∼15 nm in Pd in room temperature rolling (143), and ∼10 nm in Al in large strains and/or liquid nitrogen temperatures (24, 144). The change in twinning propensity at the nanoscale has been predominantly connected with an alteration in twinning mechanisms and the nucleation of twins from GBs (6, 24, 82, 121, 143, 144, 145). Importantly, the grain sizes seen experimentally are much larger than the corresponding w_0. This significant difference indicates that partials emitted from GBs do not behave as partials belonging to full dislocations and gliding within the grain. Hence, new models need to be developed to understand partial extension from GBs.

The critical nanograin size below which GB-driven twinning is favored has been explored numerically and analytically (129, 146–149). Some of these models calculate the critical size based on whether partial emission is preferred over full dislocation emission from GBs. However, as stated above, partial nucleation is preferred in FCC metals, and full dislocation nucleation occurs as a sequence of leading and partial emissions. Some of these models also assume that the size of the GB defect that dissociates into a partial scales with the grain size—the larger the grain size, the larger the defect and the lower the twin nucleation stress.

The critical grain size can also be based on the size below which an emitted partial dislocation from the GB can extend an SF that covers the grain cross section without nucleating the trailing partial from the same source. To demonstrate, **Figure 14a** shows a phase-field dislocation dynamics simulation in which a GB step has been inserted into the GB of a cuboidal Ni nanograin (∼60 nm). The step lies on only one atomic plane and is approximately one Burgers vector in height, much smaller than the size of the nanograin. Under an applied stress and at room temperature, a leading Shockley partial loop nucleates and expands into the grain, creating an SF in its wake (*green loop*). The SF covers a large area of the grain cross section (much greater than w_0^2) before the trailing partial nucleates (*red loop*) at the same step. As the trailing partial glides into the crystal, it removes the SF (*red*, meaning that the perfect FCC stacking sequence has been recovered). The trailing and leading partials meet, forming an extended full dislocation with w_0 nearly equaling the theoretical value; this dislocation then glides to the opposing GBs. Nucleation of the trailing partial stops twinning. Apparently, this grain size is too large to achieve even the first stage of twinning in Ni.

The simulation is repeated for Cu in **Figure 14b** using the same step and grain sizes. In this case, the leading partial can extend a SF fully across the grain cross section without nucleation of the trailing partial. This result suggests that this grain size (∼60 nm) may be sufficient for twinning in Cu. In fact, repeating this calculation for larger grain sizes shows that full traversal of the leading partial is possible for Cu grain sizes at least up to 135 nm or more for the same applied stress and step size (149). For Ni, the grain size for full traversal (using the same step size and assuming room temperature) is much smaller: only ∼7–8 nm (148). The fault energies for Ni and Cu used in the model were accounted for by incorporating the entire γ-surface calculated from DFT (**Figure 12a**).

Finally, the critical grain size is associated with the grain size at which nucleation of a second TD is favored over nucleation of the trailing partial. Zhu et al. (6, 128) applied this idea to develop an analytical model based on dislocation theory that predicts that the optimal grain sizes for twinning in nanostructured (NC) metals are ∼19–27 nm for Ni and 54 nm for Cu. Both the foregoing models therefore indicate, in agreement with experimental observations, that the nanoscale grain size for twinning is larger in Cu than in Ni.

3.3. BCC Metals

Twin in BCC metals becomes an important deformation mechanism at low temperatures and in high-strain-rate loading conditions (65, 67). The BCC TD is a partial dislocation with Burgers
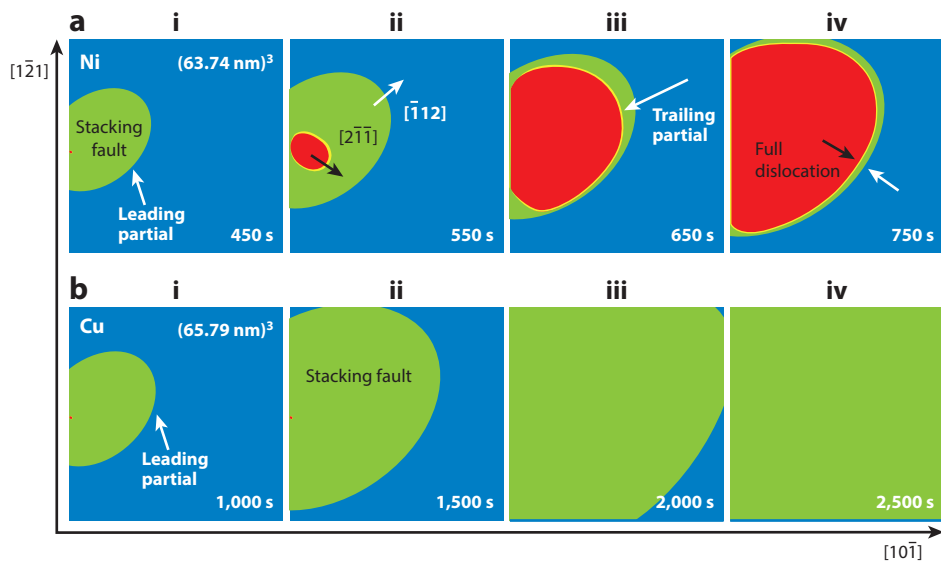
Figure 14

Density functional theory (DFT) phase field dislocation dynamics model calculations of the emission of a leading Shockley partial from a grain boundary ledge in (*a*) Ni and (*b*) Cu (148, 149). The red regions indicate that the material has slipped by a full dislocation. The green regions indicate stacking faults. In all panels, a {111} glide plane within a 3-D nanograin is visible in the plan view (with the [111] direction pointing out of the page). The first frame (*i*) of both panels *a* and *b* show the nucleation of a partial from a grain boundary defect. The leading partial leaves a stacking fault (*green*). Ni has a higher γ_I than Cu. After the leading partial propagates a certain distance into the crystal, the trailing partial nucleates from the same step [second frame (*ii*) of both panels *a* and *b*]. The trailing partial restores the FCC stacking sequence (*red*). This stops the twinning process. The leading and trailing partials form a full dislocation. (*b*) In Cu, the trailing partial is not emitted for a similar grain size (~65 nm). The model fault energies for Ni and Cu were accounted for by incorporating the entire γ-surface calculated from DFT (**Figure 12*a***).

vector (*a*/6) <111> on the {112} twin plane (3, 110). **Figure 15** shows GSFE curves for Nb for displacements along the <111> direction on the {112} plane (150). The (*a*/6) <111> displacement caused by a single TD in a perfect BCC crystal does not correspond to a local minimum on this curve. This result indicates that unlike an FCC crystal, a single TD and monolayer SF in a BCC crystal are not stable (150). Accordingly, the development of a multilayered twin nucleus cannot occur by sequential glide of identical TDs, as discussed in Section 3.2 for FCC metals. This result implies that twin nucleation mechanisms such as pole mechanisms (110, 101), which involve the glide of single layers, are not feasible. Also, pole mechanisms generally encounter other difficulties because the different model variants require energetically unfavorable reactions, such as cross-slip or the passing of two slightly separated, oppositely signed dislocations (151). For these reasons, pole mechanisms have not received experimental or numerical support for any crystal structure.

As in FCC metals, it is important to address concerns about the size of the stable twin nucleus. Numerical and experimental studies have indicated that the stable twin nucleus of a BCC twin has at least two to three layers (92–94, 99, 120, 150, 152). Christian & Mahajan (3) observed 3*n*-thick twins in BCC Mo-35%Re. One atomic-scale study (150) showed that when a monolayer SF is constructed by imposing the *a*/6[111] shear displacement corresponding to the TD, the SF transforms spontaneously into a three-layer twin. Alternatively, by using a layer-by-layer insertion
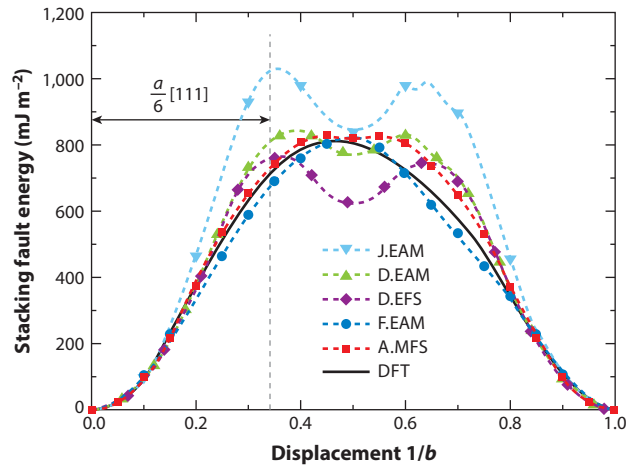
Figure 15

GSFE calculations for body-centered cubic (BCC) Nb. The GSFE curves from different interatomic potentials are compared with those calculated from DFT (*black line*). The five empirical interatomic potentials for Nb are the EAM potential developed by Johnson & Oh (J.EAM), a modified version of the Johnson-Oh potential developed by Demkowicz et al. (D.EAM), the extended Finnis-Sinclair potential by Dai et al. (D.EFS), a newly constructed force-matched EAM potential by Fellinger et al. (F.EAM), and the modified Finnis-Sinclair potential by Ackland & Thetford (A.MFS). Figure adapted from Reference 150.

method, some atomic-scale studies have calculated the change in boundary energy for twins of different layers. Results from DFT and MD using different potentials (**Figure 15**) converged for twin thicknesses of five to six layers (120, 150), which are larger than the dynamic simulation mentioned above. Interestingly, at high pressures (~50 GPa), DFT calculations (150) show that the minimum thickness for a stable nucleus becomes half the size (three layers) that it is at ambient pressures, suggesting that twinning is easier in shock conditions. This result is consistent with experimental observations (65, 67).

Another issue concerns how the twin nucleus forms. Several studies have suggested that twins in BCC metals result from dislocations. Inferring from experiments, Wasilewski (106) postulated that dislocation slip occurs before twinning and thus necessarily assists in twin formation. Sleeswyk (104) hypothesized that a three-layer twin embryo forms from the dissociation of a single screw dislocation $1/2<111>\{112\}$ into three twinning partials $1/6<111>\{112\}$ on separate planes. Ogawa (153) proposed the same outcome from the dissociation of an edge dislocation. Lagerlöf (99) based a model for the formation of the three-layer nucleus on the Sleeswyk dissociation and subsequent cross-slip of two TDs. Alternatively, Priestner & Leslie (103) proposed that these three TDs can form from the dissociation of a $<001>$ dislocation lying at the intersection of two nonplanar slip systems. In an unusual case, a series of MD simulations showed that when two coplanar, oppositely signed dislocations gliding on $\{112\}$ planes were driven toward one another at supersonic speeds, they did not annihilate but simultaneously created two more twin faults on adjacent planes. The subsequent nucleation events, in combination with the original fault, produced a three-layer twin (154). It should be kept in mind that validation via in situ observation of any twin nucleation model is difficult.

Twin thickening can proceed via a layer-by-layer process after a stable twin nucleus has formed. Lagerlöf (99) proposed that lateral propagation and thickening occur by double cross-slip of the
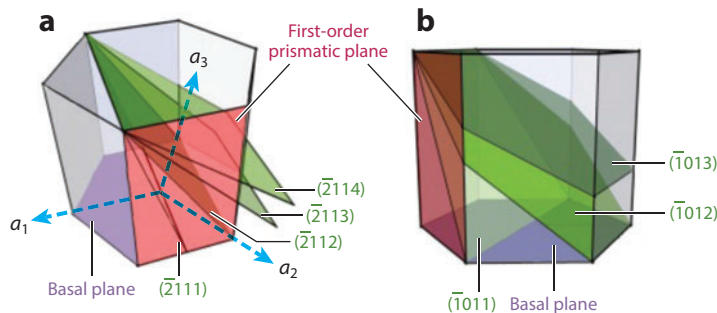
Figure 16

Seven twin modes in hexagonal close-packed (HCP) metals. The crystallography of these twin modes can also be found in References 4, 5, 96, and 114. The family of twins in panel *a* shares the common zone axis of $[0\bar{1}10]$, and the family in panel *b* shares the $[\bar{1}2\bar{1}0]$ zone axis. Figure adapted from Reference 118.

screw-oriented TDs. Mahajan (105) proposed, as another mechanism for growth, that multiple twin embryos within a slip band can coalesce to form a larger twin.

3.4. HCP Metals

The HCP metals most often studied for their structural properties and plastic deformation response are Zn, Cd, Mg, Ti, Be, Zr, and Co and their alloys (79, 88, 89, 91, 93, 112, 155). These metals commonly deform by slip and twinning in a wide range of deformation conditions. There are several modes of both slip and twinning. The main slip modes are basal $<a>$ slip, $1/3[11\bar{2}0](0001)$; prismatic $<a>$ slip, $1/3[11\bar{2}0]\{10\bar{1}0\}$; and pyramidal $<c+a>$ slip, either second-order pyramidal slip $1/3<11\bar{2}3>\{11\bar{2}2\}$ or first-order pyramidal slip $1/3<11\bar{2}3>\{10\bar{1}1\}$ (4, 5). There are at least seven twinning modes (each with six variants), with twinning planes K_1: $(\bar{2}111)$, $(\bar{2}112)$, $(\bar{2}113)$, $(\bar{2}114)$, $(\bar{1}011)$, $(\bar{1}012)$, and $(\bar{1}013)$ (**Figure 16**) and respective twinning directions η_1: $[\bar{2}11\bar{6}]$, $[\bar{2}11\bar{3}]$, $[\bar{2}11\bar{2}]$, $[\bar{4}223]$, $[\bar{1}01\bar{2}]$, $[\bar{1}01\bar{1}]$, and $[\bar{3}03\bar{2}]$. Most of these twin types have been observed in HCP metals under various deformation conditions (3–5, 117); the $\{10\bar{1}2\}$ twin occurs the most frequently (**Figure 16b**). HCP twins can take on complicated configurations: Different types of twins can form within the same grain (1, 112) (**Figure 1a**), twins can twin again internally (double twinning) (2, 109, 156) (**Figure 1b**), and these twins can twin yet again (tertiary twinning) (157). When the applied load is reversed, twin domains can revert back to the parent orientation via reverse propagation of twins [detwinning (92)] or internal twinning [retwinning (158)].

    Figure 16 shows the crystallography of these twin modes. Each twin mode is associated with an elementary TD, which is a disconnection (a zonal defect) with a dislocation character with Burgers vector *b* and a step character with height *t* (159). The step height includes *n* crystallographic planes affected by the TD. Atomic-scale simulations (160–163) have shown, for instance, that the value of *n* for the twins in **Figure 16b** is two.

    The many fundamental differences that distinguish HCP metals from cubics (e.g., FCC and BCC metals) make HCP twinning more complex, and some of the twinning concepts developed for cubics are not transferrable to HCP metals. The slip and twin modes of HCP metals correspond to planes of different atomic densities and possess different glide resistances and dislocation core configurations. These twin planes are not atomically flat but instead are rumpled or highly puckered (155, p. 970). Unlike cubic metals, the twin orientation in HCP metals cannot be completely achieved via shearing by TDs but requires supplementary atomic shuffling—atomic movements

that vary in direction and distance (155, 164, 165). Apart from a few exceptions, HCP slip planes and twin planes do not coincide.

These distinctions between HCP and cubic metals affect twin nucleation. As before, we begin with the notion that twin formation involves the dissociation of dislocations. Because the slip and twinning planes most often do not coincide, slip-to-twin dissociation reactions in HCP metals are nonplanar (**Figure 10**), and consequently, the residual dislocation b_R (Equation 4) is a stair rod. Considering the many HCP slip and twin modes, there is a large number of possible planar and nonplanar dissociation reactions. Following the dissociation rules discussed above (Section 3.1), dissociation reactions from any one of the $<a>$, $<c+a>$, or $<c>$ dislocations to one of the seven possible twins were derived in References 98 and 117 by assuming straight dislocation configurations. In most cases, the reactions were unfavorable, and stress concentrations from dislocation pileups were needed to drive these reactions. An extension of the Mendelson 2-D dissociation model to 3-D loop configurations (118) was developed later. These models show that planar dissociations are energetically favored over nonplanar dissociations and that nonplanar dissociations producing TDs on one plane are favored over those producing TDs on two or more independently oriented planes. The 3-D extension also reveals that the stress field from dislocation pileups (of ~10 dislocations) enables some reactions but not others.

Whether twinning proceeds after dissociation reactions depends on whether a stable twin nucleus can form. The structure of stable twin nuclei in HCP metals has not been explored as extensively as in cubic metals. The few studies of the seven twin types carried out thus far (107, 163) have shown that HCP twin nuclei are multilayered. Studies by Vaidya & Mahajan (107) of dislocation structures (i.e., emissary dislocations) ahead of $\{11\bar{2}1\}$ twin tips suggested a dissociation of $<c+a>$ dislocations on $\{11\bar{2}1\}$ slip planes into $\{11\bar{2}1\}$ TDs (107). On the basis of this observation, they proposed dissociation reactions involving $<a>$ and $<c+a>$ slip dislocations leading to a 12-layer $\{11\bar{2}1\}$ twin nucleus. The $\{10\bar{1}2\}$ twin has received far more attention. Recent MD work has shown that a single layer twin fault on the $(10\bar{1}2)$ plane is not stable in a perfect HCP Mg crystal (163). As discussed above for the BCC metals, the instability of a monolayer twin fault suggests that the pole mechanism for twin nucleation in HCP metals, first proposed by Thompson & Millard (100), is not possible. The MD simulations further showed that the stable $\{10\bar{1}2\}$ twin nucleus structure consists of 17 layers composed of different dislocations whose net Burgers vector equals that of the TD (163).

Although twin nucleation may initiate with dislocation dissociations and may end with multilayered nuclei, there is still the question of what happens in between; that is, how do the multilayered nuclei form? In HCP metals, glide of TDs on preexisting TBs is accommodated by a mix of shear and shuffling of the atoms (shear-shuffle mode) (110). This same shear-shuffle process, however, may not apply to the introduction of a twin nucleus in a perfect crystal (e.g., with no preexisting TB). This issue has been addressed over the years for the common HCP $\{10\bar{1}2\}$ twin. Le Lann & Dubertret (164) proposed that the displacements of the atoms involved in reorienting the crystal to twin orientation are realized via atomic shuffling (pure shuffling). In their description, shuffling enables the basal plane in the crystal to transform into the prismatic plane in the twin. Since this study, indirect experimental evidence, such as the presence of prismatic/basal boundaries and the lack of emissary dislocations (166), has supported a pure-shuffle model for $\{10\bar{1}2\}$ twinning. MD simulations have provided numerical evidence of pure shuffling (76, 167, 168). In these MD studies, twin formation was triggered differently: production of TD dipoles on preexisting TBs (167), dissociation of a dislocation dipole inserted into a perfect crystal (168), and dissociation of GB dislocations (76, 114). However, the pure-shuffle nucleation model appeared valid in all studied cases.

The atomic-scale study by Wang et al. (76) enabled the stages of nucleation to be captured in detail for the first time. **Figure 17** illustrates the method of formation. Twin nucleation is
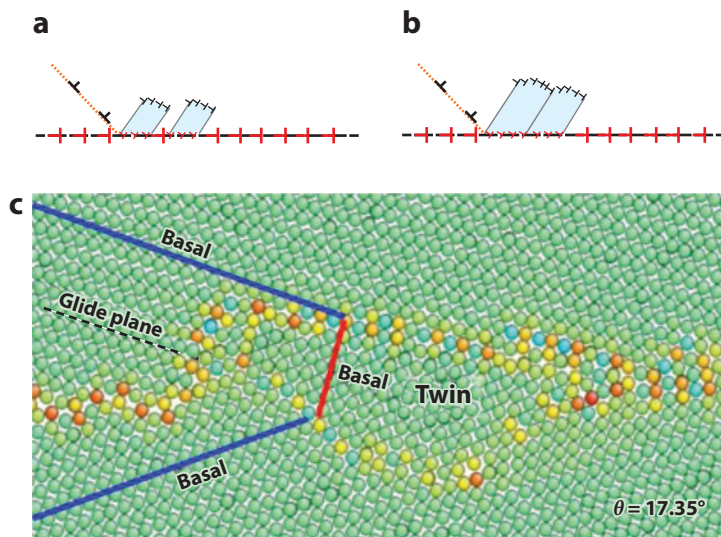

Stair rod: partial dislocation that lies along the intersection line of two glide planes; can form when two nonplanar dislocations interact, from a nonplanar dislocation dissociation, or when a dissociated dislocation extends onto another glide plane

Emissary dislocations: full dislocations emitted from a twin front to reduce the long-range stress field produced by the twin front

Figure 17

Formation of a {10$\bar{1}$2} twin embryo in a grain boundary. (*a*) <*a*> basal dislocations intersect the boundary. (*b*) Upon absorption, the grain boundary dislocations dissociate, resulting in the formation of several small embryos of twin orientation. (*c*) The embryos coalesce into a larger embryo. The atoms are colored according to a central symmetry analysis. All panels are adapted with permission from Wang et al. (114).

triggered when a basal dislocation pileup intersects a GB containing an array of GB dislocations. These GB dislocations do not correspond to lattice dislocations (76, 114). As the dislocations run into the GB, several GB dislocations dissociate, forming small embryos via pure atomic shuffling along the GB plane (76). In time, these embryos expand and coalesce into a single, larger embryo. Eventually, the nucleus propagates into the upper crystal, forming a {10$\bar{1}$2} twin. According to DFT calculations (76), the associated transformation stresses are large (∼3 GPa), supporting the notion that GBs, where high stresses and heterogeneities are located, are preferred sites for HCP twinning. Interestingly, these results suggest another distinction between twins in HCP metals and cubic metals—unlike twin nuclei in cubic metals, the {10$\bar{1}$2} twin nucleus is not constructed by adjacent layers of TDs.

As in metals with cubic crystal structures, grain size and alloying elements have been observed to affect twinning in HCP metals (67, 169, 170). However, we are just beginning to develop a mechanistic understanding via modeling, largely with the use of DFT (e.g., 171).

Twin nucleation studies have been less comprehensive for the other HCP twin modes. For the nucleation of a {10$\bar{1}$1} twin, for instance, both pure-shuffle (165) and shear-shuffle (172) mechanisms have been proposed. A dissociation-based nucleation model for secondary {10$\bar{1}$2} twins within {10$\bar{1}$1} or {10$\bar{1}$3} twins (i.e., double twinning) was put forward in Reference 109. Clearly, much more work needs to be performed to elucidate the processes underlying the nucleation of other twin modes; for instance, do the number of layers in a stable twin nucleus vary depending on alloying or twin type?

Although it is not a mechanism for twin nucleus formation, a single TD is stable on a preexisting TB; hence, layer-by-layer glide of TDs is a possible mechanism for twin thickening (160–162). Sequential glide of single TDs on a TB can thicken or shrink an existing HCP twin. Many possible sources of these TDs have been examined. They can be emitted from GBs via dissociations of GB dislocations, or they can nucleate on preexisting TBs under high-stress states (167, 168, 172). They

can also form as a result of dissociations of lattice dislocations that run into the TB (137, 160–162). The dissociation produces a TD (disconnection) of the same variant as the TB and an immobile residual dislocation b_R (Equation 4). The n-layer-thick TD glides away from the reaction site, advancing or shrinking the TB by n layers. This mechanism for TB migration applies in principle to all twins (98, 110) and has been seen in simulation for many twin modes (137, 160–162).

3.5. Twinning from Bimetal Interfaces

Nanostructured composites, in which one or more of the phases have nanoscale dimensions, have attracted much interest as they have been proven to outperform their constituents in strength and hardness (173–176), thermal stability (174–176), high strain rate or shock response (177), and radiation resistance (175, 178) by at least an order of magnitude. These composites combine two immiscible metals and, as nanostructures, contain an unusually high density of bimetal interfaces. In many recent studies, the bimetal interfaces are found to play an important role in twin formation, serving as a source of TDs. Bimetal interfaces can result in uncommon twinning behavior not seen in their nanostructured constituents.

We first consider the Ag-Cu material system deformed at room temperature. This system combines a material that twins easily at room temperature [Ag with a low γ_I (see **Figure 12a**)] with one that does not (Cu with a medium γ_I). Experimental studies have reported twinning in both the Ag and Cu phases within severely deformed Ag-Cu composites. In cold-wire-drawn Ag-Cu filaments, twins in both Ag and Cu were seen emanating from Ag-Cu interfaces (179–181). Similarly, fine Ag and Cu twins were observed from Ag-Cu interfaces in an Ag-Cu eutectic nanocomposite developed after warm rolling (150–200°C) to 75% reduction (1.6 strain) (141). In both cases, twinning in Cu was not expected. The latter study measured the texture and interface character before and after deformation (141). Both measurements indicated that twinning was not limited to the fine twins seen in the microscope after deformation but rather that twinning occurred profusely during deformation: a twin volume fraction of at least 30% was achieved in both the Ag and Cu phases. X-ray diffraction texture measurements showed that the deformation textures of Cu and Ag were nearly alike and corresponded to the rolling texture of an FCC material that had generated a twin volume fraction of at least 30% (**Figure 18a**). TEM analyses of interface character indicated that the Ag-Cu interfaces had transformed from their initial {111} interface plane to a {001} plane (**Figure 18b**) while maintaining a cube-on-cube orientation relationship. This alteration in interface character results when twins cross the interface, causing the interface plane to reorient. **Figure 18c** shows the underlying sequence of events as seen in MD simulations: Ag TDs first impinge on the interface, then become absorbed, and finally dissociate into Cu TDs that emit into Cu. Each time a TD transmits in this way, the interface plane reorients from {111} to {001}, and a residual dislocation b_R is left in the interface (**Figure 18c**) (182). Accordingly, as the Ag phase twins, the Cu phase can twin alongside it via sequential Ag-TD absorption and Cu-TD emission on adjacent glide planes. As the Ag and Cu twins thicken, residual dislocations accumulate within the interface, increasing the interface energy. Wang et al. (182) proposed that to reduce the interface energy, these residuals rearrange into larger steps that subsequently dissociate into very fine twins or layers of SFs. This explains the observation of fine Ag and Cu twins seen emanating from the {001} cube-on-cube bimetal interface after deformation.

Deformation twinning has also been studied in Cu-Nb composites (115, 116, 181, 183). Unlike Ag-Cu composites, Cu-Nb composites join two metals that do not twin easily at room temperature or at quasi-static rates (see Sections 3.2 and 3.3). However, as discussed in Section 3.2, nanograin sizes can promote twinning in single-phase Cu but not Nb in these conditions. Thus, in a nanostructured Cu-Nb composite, the Cu phase could twin if the grains were sufficiently fine
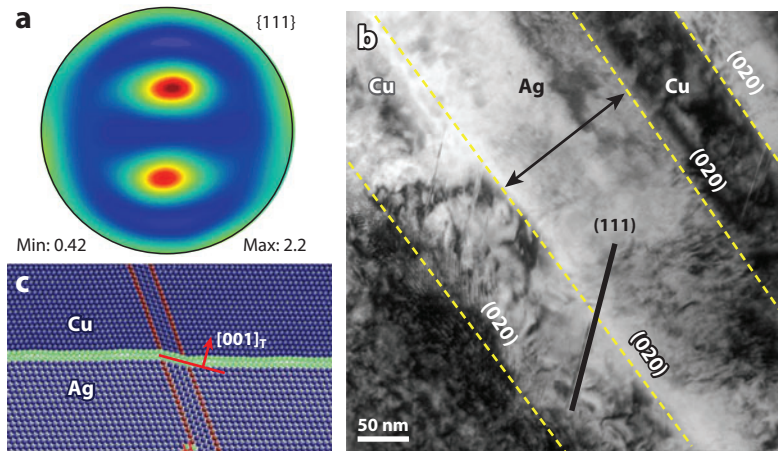
Interface character:
a five-parameter geometric property describing the orientation relationship of the two crystals on either side of the interface and the interface plane

Cube-on-cube:
a special orientation relationship between two crystals in which all crystallographic axes of the two crystals are parallel

Figure 18

(*a*) A {111} pole figure of the typical texture of the Cu and Ag phases in a nanolayered eutectic composite after rolling to 75% rolling reduction under either room temperature or elevated temperature. Panel *a* adapted from Reference 176. The colors indicate intensity in units of multiples of random distribution (mrd). Blue is 1.0 mrd, and red is 2.0 mrd. (*b*) TEM micrograph of the material after rolling showing a change in the interface plane to {001}. (*c*) MD simulation of Ag-to-Cu twin-twin transmission, in which the transmission reorients the interface. The subscripted T corresponds to the coordinates in the twinned crystal. The atoms are colored according to a central symmetry analysis. Panel *c* adapted from Reference 182.

(e.g., <150 nm) (70, 83, 141). Some studies support this hypothesis. **Figure 19** shows the progression of twinning in the Cu phase as a bulk sheet of Cu-Nb nanolayered composite is rolled (the rolling direction is the horizontal direction in the figure). Increasing the applied rolling strain causes the layer thickness h to decrease from 135 to 10 nm and concomitantly causes the frequency of twinning in Cu to increase from <5% to ~30% (115, 116). Likewise, Cu twins have also been observed in wire-drawn, nanostructured Cu-Nb filaments in the vicinity of the Cu-Nb interfaces (181). However, in other studies, deforming nanostructured Cu-Nb composites did not lead to twinning. Thin films of Cu-Nb nanolayered composites made by deposition and possessing similar fine, nanosized (<50 nm) length scales did not twin under the same conditions as in **Figure 19** (183). In fact, even under more severe conditions (high rates) or other deformation modes (e.g., shear, tensile testing), the Cu phase in these nanolayered Cu-Nb films did not twin. Likewise, subjecting the Cu-Nb nanocomposite sheets (layer thickness $h \leq 60$ nm) in **Figure 19** to a strain path change (transverse rolling) suppressed twinning (173). The bimetal interfaces in each of these composites—unidirectionally rolled, transverse rolled, and deposited films—had different interface characters (173, 183–185). Evidently, for two-phase materials, grain size and crystal orientation are not the only factors affecting twinning; the properties of the interfaces also appear to govern whether twinning occurs.

In the cases in which twins were observed, they clearly originated from the bimetal interfaces. In **Figure 19*b***, a high-resolution TEM (HRTEM) image shows an example of a twin emanating from the {112}<110>Cu∥{112}<111>Nb interface (186) in the bulk Cu-Nb sheet. Because the Cu grain twins but the adjacent Nb grain does not, the character of their common Cu-Nb interface has changed. This figure shows that, within the twin domain, the interface has reoriented to {552}<110>Cu∥{112}<111> Nb. Despite the alteration in interface character, the interface remains flat both before and after twinning. This suggests that the twin shown was constructed of TDs with different Burgers vectors such that the net Burgers vector is zero, much like the
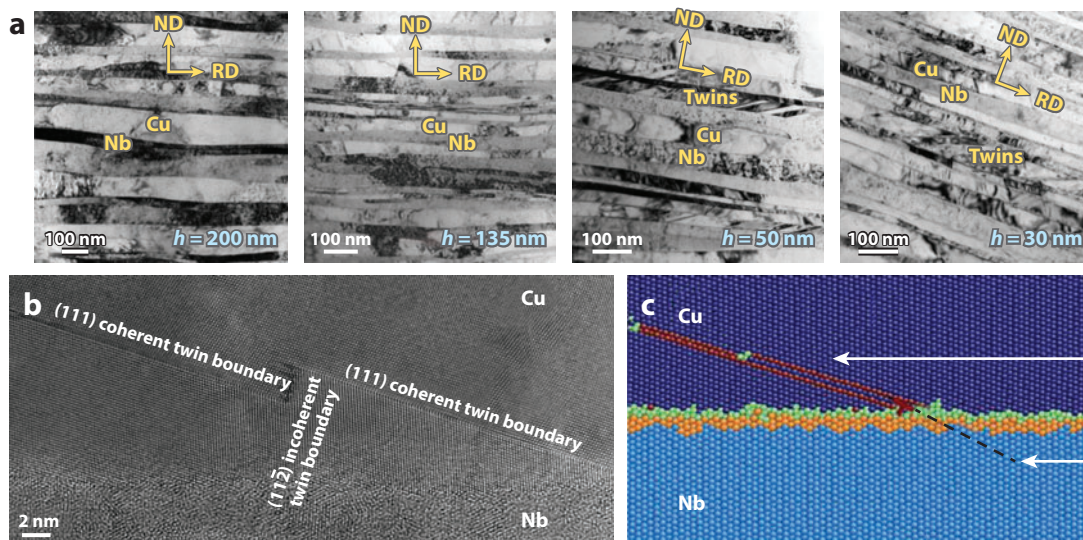
Figure 19

(*a*) Development of deformation twins in the Cu phase in a Cu-Nb nanolayered composite. ND denotes the normal direction, RD denotes the rolling direction, and h denotes the layer thickness. (*b*) TEM micrograph showing a twin connected to a Cu-Nb interface. The interface is {112}<110>Cu‖{112}<111>Nb, which is characteristic of this material (184, 185). Panel *b* adapted from Reference 186. (*c*) MD simulation of slip-twin transmission from Nb to Cu, preferentially creating a twin on the same twin plane observed experimentally. Adapted with permission from Reference 188. The arrows point to the incoming slip plane and outgoing twin plane.

zero-strain twinning mechanisms proposed for single-phase FCC metals (108, 135) (see Section 3.2). As evidence, **Figure 19*b*** shows the emission of a group of partials from the Cu-Nb interface with a vertical, incoherent $\Sigma 3$ twin front, indicating that this group had a net Burgers vector of zero. Because these types of twins do not accommodate strain, it is doubtful that all twins in this material are zero-strain twins. In support, a recent TEM analysis suggested that the residual dislocations accumulated after twin formation at a Cu-Nb interface rearranged to a lower-energy, flat morphology (188).

Zheng et al. (116) carried out in situ nanoindentation in the TEM on this Cu-Nb material. This study provided further evidence that twins are emitted from the bimetal interfaces on both sides of the grain; it also revealed an interesting thickening mechanism. Twin formation began by the nucleation of two fine twins separated by ~10 nm in the same crystal. Subsequently, the crystal in between twinned entirely by the emission of fine twins from the two opposing interfaces on either side of the crystal. The result is a ~10-nm-thick twin. Thick twins formed in this way are unlike the fine twins typically seen in monolithic Cu (66).

Taken together, the above results indicate that in nanostructured composites with nanosized grains, the bimetal interfaces are the primary sources of TDs (115, 116, 141, 182, 186). Both nucleation and growth of twins can occur via sequences of TD emissions from the bimetal interface.

In light of the fact that Cu-Nb nanocomposites with different interface characters do not exhibit the same twinnabilities, the next issue that arises is how the character of an interface affects its ability to provide TDs. Under deformation, dislocations within the bimetal interface can dissociate into TDs that are then emitted into the crystal. In the Ag-Cu system, we find that the Ag TDs can supply Cu TDs provided they can transmit across the bimetal interface. Because Nb does not twin but deforms by slip in the Cu-Nb system, two other possible mechanisms are considered.

Interface dislocations from which TDs may be emitted (*a*) may already exist in the interface as intrinsic (misfit) dislocations (187) or (*b*) may have resulted from interactions with run-in Nb slip dislocations (115, 188) (**Figure 19c**). Using MD simulations and dislocation theory, a recent study explored the relationship between the character of an interface and its ability to act as a source of TDs in these two ways (115). The predominant interface character in the bulk sheet composites in **Figure 19** contains intrinsic interface dislocations with nonplanar Burgers vectors that can dissociate into TDs. Likewise, this particular interface is resistant to interfacial sliding. Thus, when a Nb dislocation approaches the interface, it can more easily become absorbed and emit into the Cu side, as seen in MD simulations (**Figure 19c**). Because both interfacial sources of TDs can be supplied by this interface, deformation twinning in the Cu phase is likely. In contrast, the characteristic interface in the physical-vapor-deposited Cu-Nb foils—the Kurdjumov-Sachs interface {111}<110>Cu∥{110}<111>Nb or the Nishiyama-Wasserman interface (184, 185)—has interface dislocations with planar Burgers vectors and a low shear resistance. These interface characters have a limited ability to act as a source of TDs, explaining why twins are not seen in these Cu-Nb deposited thin films under all deformation modes and conditions.

These few studies on Ag-Cu and Cu-Nb composites reveal that it is possible to change the twinnability of a material by tuning its interface character. More studies on engineering bimetal interfaces are recommended.

SUMMARY POINTS

1. Vapor- or electrodeposition of low- to medium-SF-energy FCC metals and alloys can be used to synthesize NT structures with an average twin lamella thickness of <10 nm. NT structures exhibit unusually high hardness and strengths along with good deformability.

2. Because the energy of a TB is lower than that of a high-angle GB, NT structures exhibit very high thermal stability and much better retention of strength after annealing compared with their NC counterparts.

3. Twin nuclei in the three crystal structures reviewed here (FCC, BCC, and HCP) are multilayered. A twin nucleus forms from dislocations, and the mechanisms require high stress. Once a stable nucleus has formed, it can grow by layer-by-layer glide of TDs.

4. The twin nucleation mechanisms of many of the seven observed HCP twin types have yet to be explored.

5. Twins preferentially form from GBs and bimetal interfaces. The atomic- and nanoscale features of these boundaries and interfaces profoundly affect the ability of a material to form deformation twins.

DISCLOSURE STATEMENT

The authors are not aware of any affiliations, memberships, funding, or financial holdings that might be perceived as affecting the objectivity of this review.

ACKNOWLEDGMENTS

LITERATURE CITED

1. McCabe RJ, Proust G, Cerreta EK, Misra A. 2009. Quantitative analysis of deformation twinning in zirconium. *Int. J. Plast.* 25:454–72
2. Capolungo L, Marshall PE, McCabe RJ, Beyerlein IJ, Tomé CN. 2009. Nucleation and growth of twins in Zr: a statistical study. *Acta Mater.* 57:6047–56
3. Christian JW, Mahajan S. 1995. Deformation twinning. *Prog. Mater. Sci.* 39:1–157
4. Partridge PG. 1967. The crystallography and deformation modes of hexagonal close-packed metals. *Metall. Rev.* 12:168–94
5. Yoo MH, Morris JR, Ho KM, Agnew SR. 2002. Nonbasal deformation modes of HCP metals and alloys: role of dislocation source and mobility. *Metall. Mater. Trans. A* 33:813–22
6. Zhu YT, Liao XZ, Wu XL. 2012. Deformation twinning in nanocrystalline materials. *Prog. Mater. Sci.* 57:1–62
7. Mahajan S. 2013. Critique of mechanisms of formation of deformation, annealing and growth twins: face-centered cubic metals and alloys. *Scr. Mater.* 68:95–99
8. Bouaziz O, Allain S, Scott CP, Cugy P, Barbier D. 2011. High manganese austenitic twinning induced plasticity steels: a review of the microstructure properties relationships. *Curr. Opin. Solid State Mater. Sci.* 15:141–68
9. Mahajan S, Pande CS, Imam MA, Rath BB. 1997. Formation of annealing twins in FCC crystals. *Acta Mater.* 45:2633–38
10. Barsch GR, Horovitz B, Krumhansl JA. 1987. Dynamics of twin boundaries in martensites. *Phys. Rev. Lett.* 59:1251–54
11. De Cooman BC. 2004. Structure–properties relationship in TRIP steels containing carbide-free bainite. *Curr. Opin. Solid State Mater. Sci.* 8:285–303
12. Field RD, McCabe RJ, Alexander DJ, Teter DF. 2009. Deformation twinning and twinning related fracture in coarse-grained α-uranium. *J. Nucl. Mater.* 392:105–13
13. Simha NK. 1997. Twin and habit plane microstructures due to the tetragonal to monoclinic transformation of zirconia. *J. Mech. Phys. Solids* 45:261–63, 265–92
14. Lu L, Shen YF, Chen XH, Qian LH, Lu K. 2004. Ultrahigh strength and high electrical conductivity in copper. *Science* 304:422–26
15. Lu L, Chen X, Huang X, Lu K. 2009. Revealing the maximum strength in nanotwinned copper. *Science* 323:607–10
16. Lu K, Lu L, Suresh S. 2009. Strengthening materials by engineering coherent internal boundaries at the nanoscale. *Science* 324:349–52
17. Zhang X, Misra A, Nastasi M, Hoagland RG. 2006. Preparation of high-strength nanometer-scale twinned coating and foil. *US Patent No. 7,078,108*
18. Zhang X, Misra A, Wang H, Nastasi M, Embury JD, et al. 2004. Nanoscale-twinning-induced strengthening in austenitic stainless steel thin films. *Appl. Phys. Lett.* 84:1096–98
19. Zhang X, Wang H, Chen XH, Lu L, Lu K, et al. 2006. High-strength sputter-deposited Cu foils with preferred orientation of nanoscale growth twins. *Appl. Phys. Lett.* 88:173116
20. Bufford D, Wang H, Zhang X. 2011. High strength, epitaxial nanotwinned Ag films. *Acta Mater.* 59:93–101

21. Wang JG, Tian ML, Mallouk TE, Chan MHW. 2004. Microtwinning in template-synthesized single-crystal metal nanowires. *J. Phys. Chem. B* 108:841–45

22. Zhang X, Misra A. 2012. Superior thermal stability of coherent twin boundaries in nanotwinned metals. *Scr. Mater.* 66:860–65

23. Anderoglu O, Misra A, Zhang X. 2008. Epitaxial nanotwinned Cu films with high strength and high conductivity. *Appl. Phys. Lett.* 93:083108

24. Wang YM, Sansoz F, LaGrange T, Ott RT, Marian J, et al. 2013. Defective twin boundaries in nano-twinned metals. *Nat. Mater.* 12:697–702

25. Jang DC, Li X, Gao H, Greer JR. 2012. Deformation mechanisms in nanotwinned metal nanopillars. *Nat. Nanotechnol.* 7:594–601

26. Wang J, Sansoz F, Huang J, Liu Y, Sun S, et al. 2013. Near-ideal theoretical strength in gold nanowires containing angstrom scale twins. *Nat. Commun.* 7:1742

27. Anderoglu O, Zhang X, Misra A. 2008. Thermal stability of sputtered Cu films with nanoscale growth twins. *J. Appl. Phys.* 103:094322

28. Zhao YF, Furnish TA, Kassner ME, Hodge AM. 2012. Thermal stability of highly nanotwinned copper: the role of grain boundaries and texture. *J. Mater. Res.* 27:3049–57

29. Jin ZH, Gumbsch P, Ma E, Albe K, Lu K, et al. 2006. The interaction mechanism of screw dislocations with coherent twin boundaries in different face-centred cubic metals. *Scr. Mater.* 54:1163–68

30. Zhang X, Misra A, Wang H, Lima AL, Hundley MF, Hoagland RG. 2005. Effects of deposition parameters on residual stresses, hardness and electrical resistivity of nanoscale twinned 330 stainless steel thin films. *J. Appl. Phys.* 97:094302

31. Deng C, Sansoz F. 2009. Enabling ultrahigh plastic flow and work hardening in twinned gold nanowires. *Nano Lett.* 9:1517–22

32. Li X, Wei Y, Lu L, Lu K, Gao H. 2010. Dislocation nucleation governed softening and maximum strength in nano-twinned metals. *Nature* 464:877–80

33. Wang J, Li N, Anderoglu O, Zhang X, Misra A, et al. 2010. Detwinning mechanisms for growth twins in face-centered cubic metals. *Acta Mater.* 58:2262–70

34. Hodge AM, Furnish TA, Shute CJ, Liao Y, Huang X, et al. 2012. Twin stability in highly nanotwinned Cu under compression, torsion and tension. *Scr. Mater.* 66:872–77

35. Wu ZX, Zhang YW, Srolovitz DJ. 2011. Deformation mechanisms, length scales and optimizing the mechanical properties of nanotwinned metals. *Acta Mater.* 59:6890–900

36. You Z, Li X, Gui L, Lu Q, Zhu T, et al. 2013 Plastic anisotropy and associated deformation mechanisms in nanotwinned metals. *Acta Mater.* 61:217–27

37. Bufford D, Wang H, Zhang X. 2013. Thermal stability of twins and strengthening mechanisms in differently oriented epitaxial nanotwinned Ag films. *J. Mater. Res.* 28:1729–39

38. Pharr GM, Oliver WC. 1989. Nanoindentation of silver-relations between hardness and dislocation structure. *J. Mater. Res.* 4(1):94–101

39. Christopher D, Smith R, Richter A. 2001. Atomistic modelling of nanoindentation in iron and silver. *Nanotechnology* 12(3):372

40. Zhao MH, Slaughter WS, Li M, Mao SX. 2003. Material-length-scale-controlled nanoindentation size effects due to strain-gradient plasticity. *Acta Mater.* 51(15):4461–69

41. Panin AV, Shugurov AR, Oskomov KV. 2005. Mechanical properties of thin Ag films on a silicon substrate studied using the nanoindentation technique. *Phys. Solid State* 47(11):2055–59

42. Cao Y, Allameh S, Nankivil D, Sethiaraj S, Otiti T, Soboyejo W. 2006. Nanoindentation measurements of the mechanical properties of polycrystalline Au and Ag thin films on silicon substrates: effects of grain size and film thickness. *Mater. Sci. Eng. A* 427(1–2):232–40

43. Fu YQ, Shearwood C, Xu B, Yu LG, Khor KA. 2010. Characterization of spark plasma sintered Ag nanopowders. *Nanotechnology* 21(11):115707

44. Gu P, Dao M, Asaro RJ, Suresh S. 2011. A unified mechanistic model for size-dependent deformation in nanocrystalline and nanotwinned metals. *Acta Mater.* 59:6861–68

45. Chen XH, Lu L, Lu K. 2007. Electrical resistivity of ultrafine-grained copper with nanoscale growth twins. *J. Appl. Phys.* 102:083708

46. Anderoglu O, Misra A, Ronning F, Zhang X. 2009. Significant enhancement of the strength-to-resistivity ratio by using nanotwins in epitaxial Cu films. *J. Appl. Phys.* 106:024313
47. Chen KC, Wu WW, Liao CN, Chen LJ, Tu KN. 2010. Stability of nanoscale twins in copper under electric current stressing. *J. Appl. Phys.* 108:066103
48. Qian LH, Lu QH, Kong WJ, Lu K. 2004. Electrical resistivity of fully-relaxed grain boundaries in nanocrystalline Cu. *Scr. Mater.* 50:1407–11
49. Cui BZ, Han K, Xin Y, Waryoba DR, Mbaruku AL. 2007. Highly textured and twinned Cu films fabricated by pulsed electrodeposition. *Acta Mater.* 55:4429–38
50. Han K, Walsh RP, Ishmaku A, Toplosky V, Brandao L, Embury JD. 2004. High strength and high electrical conductivity bulk Cu. *Philos. Mag.* 84:3705–16
51. Chang SC, Shieh JM, Fang JY, Wang YL, Dai BT, Feng MS. 2004. Roles of copper mechanical characteristics in electropolishing. *J. Vac. Sci. Technol. B* 22:116
52. Dahlgren SD, Nicholson WL, Merz MD, Bollmann W, Devlin JF, Wang R. 1977. Microstructural analysis and tensile properties of thick copper and nickel sputter deposits. *Thin Solid Films* 40:345–53
53. Bhattacharyya D, Liu XY, Genc A, Fraser HL, Hoagland RG, Misra A. 2010. Heterotwin formation during growth of nanolayered Al-TiN composites. *Appl. Phys. Lett.* 96:093113
54. Bhattacharyya D, Mara NA, Dickerson P, Hoagland RG, Misra A. 2011. Compressive flow behavior of Al-TiN multilayers at nanometer scale layer thickness. *Acta Mater.* 59:3804–16
55. Bufford D, Liu Y, Zhu Y, Bi Z, Jia QX, et al. 2013. Formation mechanisms of high-density growth twins in aluminum with high stacking-fault energy. *Mater. Res. Lett.* 1:51–60
56. Bufford D, Bi Z, Jia QX, Wang H, Zhang X. 2012. Nanotwins and stacking faults in high-strength epitaxial Ag/Al multilayer films. *Appl. Phys. Lett.* 101:223112
57. Liu Y, Bufford D, Wang H, Sun C, Zhang X. 2011. Mechanical properties of highly textured Cu/Ni multilayers. *Acta Mater.* 59:1924–33
58. Zhang ZY, Li FY, Ma GJ, Kang RK, Guo XG. 2013. Ultrahigh hardness and improved ductility for nanotwinned mercury cadmium telluride. *Scr. Mater.* 69:231–34
59. Tian YJ, Xu B, Yu DL, Ma YM, Wang YB, et al. 2013. Ultrahard nanotwinned cubic boron nitride. *Nature* 493:385–88
60. Wang HT, Tao NR, Lu K. 2012. Strengthening an austenitic Fe-Mn steel using nanotwinned austenitic grains. *Acta Mater.* 60:4027–40
61. Frontan J, Zhang YM, Dao M, Lu J, Galvez F, Jerusalem A. 2012. Ballistic performance of nanocrystalline and nanotwinned ultrafine crystal steel. *Acta Mater.* 60:1353–67
62. Yuan Y, Gu YF, Osada T, Zhong ZH, Yokokawa T, Harada H. 2012. A new method to strengthen turbine disc superalloys at service temperatures. *Scr. Mater.* 66:884–89
63. Demkowicz MJ, Anderoglu O, Zhang X, Misra A. 2011. The influence of Σ3 twin boundaries on the formation of radiation-induced defect clusters in nanotwinned Cu. *J. Mater. Res.* 26:1666–75
64. Yu KY, Bufford D, Sun C, Liu Y, Wang H, et al. 2013. Removal of stacking-fault tetrahedra by twin boundaries in nanotwinned metals. *Nat. Commun.* 4:1377
65. Huang JC, Gray GT III. 1989. Microband formation in shock-loaded and quasi-statically deformed metals. *Acta Metall.* 37:3335–47
66. Cao F, Beyerlein IJ, Addessio FL, Sencer BH, Trujillo CP, et al. 2010. Orientation dependence of shock induced twinning and substructures in a copper bicrystal. *Acta Mater.* 58:549–59
67. Gray GT III. 2012. High-strain-rate deformation: mechanical behavior and deformation structures induced. *Annu. Rev. Mater. Res.* 42:285–303
68. Smith CS. 1958. Metallographic studies of metals after explosive shock. *Trans. Metall. Soc. AIME* 212:574–89
69. Gray GT III. 1988. Deformation twinning in Al-4.8 wt% Mg. *Acta Metall.* 36:1745–54
70. Zhao WS, Tao NR, Guo JY, Lu QH, Lu K. 2005. High density nano-scale twins in Cu induced by dynamic plastic deformation. *Scr. Mater.* 53:745–49
71. Blewitt TH, Coltman RR, Redman JK. 1957. Low-temperature deformation of copper single crystals. *J. Appl. Phys.* 28:651
72. Niezgoda SR, Kanjarla AK, Beyerlein IJ, Tomé CN. 2014. Stochastic modeling of twin nucleation in polycrystals: an application in hexagonal close-packed metals. *Int. J. Plast.* 56:119–38

73. Brown DW, Beyerlein IJ, Sisneros TA, Clausen B, Tomé CN. 2012. Role of deformation twinning and slip during compressive deformation of beryllium as a function of strain rate. *Int. J. Plast.* 29:120–35

74. Beyerlein IJ, Capolungo L, Marshall PE, McCabe RJ, Tomé CN. 2010. Statistical analyses of deformation twinning in magnesium. *Philos. Mag.* 90:2161–90

75. Pond RC, Garcia-Garcia LMF. 1982. Deformation twinning in aluminum. In *Electron Microscopy and Analysis*, ed. MJ Goringe, pp. 495–98. Bristol, UK: IOP

76. Wang J, Yadav SK, Hirth JP, Tomé CN, Beyerlein IJ. 2013. Pure-shuffle nucleation of deformation twins in hexagonal-close-packed metals. *Mater. Res. Lett.* 1:126–32

77. Beyerlein IJ, Tóth LS, Tomé CN, Suwas S. 2007. Role of twinning on texture evolution of silver during equal channel angular extrusion. *Philos. Mag.* 87:885–906

78. Adams BL, Fullwood DT, Basinger J, Hardin T. 2012. High resolution EBSD-based dislocation microscopy. *Mater. Sci. Forum* 702–3:11–17

79. Beyerlein IJ, McCabe RJ, Tomé CN. 2011. Stochastic processes of {1012} deformation twinning in hexagonal close-packed polycrystalline zirconium and magnesium. *Int. J. Multiscale Comput. Eng.* 9:459–80

80. Wang L, Eisenlohr P, Yang Y, Bieler TR, Crimp MA. 2010. Nucleation of paired twins at grain boundaries in titanium. *Scr. Mater.* 63:827–30

81. Wang L, Yang Y, Eisenlohr P, Bieler TR, Crimp MA, Mason DE. 2010. Twin nucleation by slip transfer across grain boundaries in commercial purity titanium. *Metall. Mater. Trans.* 41:421–30

82. Liao XZ, Srinivasan SG, Zhao YH, Baskes MI, Zhu YT. 2004. Formation mechanism of wide stacking faults in nanocrystalline Al. *Appl. Phys. Lett.* 84:3564–66

83. Yue Y, Liu P, Deng Q, Ma E, Zhang Z, Han X. 2012. Quantitative evidence of crossover toward partial dislocation mediated plasticity in copper single crystalline nanowires. *Nano Lett.* 12:4045–49

84. Yu Q, Qi L, Chen K, Mishra RK, Li J, Minor AM. 2012. The nanostructured origin of deformation twinning. *Nano Lett.* 12:887–92

85. Reed-Hill RE. 1964. Role of deformation twinning in the plastic deformation of a polycrystalline anisotropic metal. In *Deformation Twinning*, ed. RE Reed-Hill, JP Hirth, HC Rogers, pp. 295–320. Gainesville, FL: Gordon & Breach

86. Tomé CN, Maudlin PJ, Lebensohn RA, Kaschner GC. 2001. Mechanical response of zirconium—I. Derivation of a polycrystal constitutive law and finite element analysis. *Acta Mater.* 49:3085–96

87. El Kadiri H, Oppedal AL. 2010. A crystal plasticity theory for latent hardening by glide twinning through dislocation transmutation and twin accommodation effects. *J. Mech. Phys. Solids* 58:613–24

88. Salem AA, Kalidindi SR, Doherty RD, Semiatin SL. 2006. Strain hardening due to deformation twinning in α-titanium: mechanisms. *Metall. Mater. Trans. A* 37:259–68

89. Proust G, Tomé CN, Jain A, Agnew SR. 2009. Modeling the effect of twinning and detwinning during strain-path changes of magnesium alloy AZ31. *Int. J. Plast.* 25:861–80

90. Sriram V, Yang JM, Jia Y, Minor AM. 2008. Determining the stress required for deformation twinning in nanocrystalline and ultrafine-grained copper. *JOM* 60:66–70

91. Al-Maharbi M, Karaman I, Beyerlein IJ, Foley D, Hartwig KT, et al. 2011. Microstructure, crystallographic texture, and plastic anisotropy evolution in an Mg alloy during equal channel angular extrusion processing. *Mater. Sci. Eng. A* 528:7616–27

92. Knezevic M, Beyerlein IJ, Brown DW, Sisneros TA, Tomé CN. 2013. A polycrystal plasticity model for predicting mechanical response and texture evolution during strain-path changes: application to beryllium. *Int. J. Plast.* 49:185–98

93. Agnew SR, Tomé CN, Brown DW, Holden TM, Vogel SC. 2003. Study of slip mechanisms in a magnesium alloy by neutron diffraction and modeling. *Scr. Mater.* 48:1003–8

94. Orowan E. 1954. Dislocations and mechanical properties. In *Dislocations in Metals*, ed. M Cohen, pp. 69–195. New York: Am. Inst. Mining Metall. Eng.

95. Lee JK, Yoo MH. 1992. Theory of shape bifurcation during nucleation in solids. *Metall. Trans. A* 23:1891–900

96. Yoo MH, Lee JK. 1991. Deformation twinning in h.c.p. metals and alloys. *Philos. Mag.* 63:987–1000

97. Cohen JB, Weertman J. 1963. A dislocation model for twinning in FCC metals. *Acta Metall.* 11:997

98. Yoo MH. 1969. Interaction of slip dislocations with twins in HCP metals. *Trans. Metal Soc. AIME* 245:2051–60

99. Lagerlöf KPD. 1993. On deformation twinning in B.C.C. metals. *Acta Metall. Mater.* 41:2143–51

100. Thompson N, Millard DJ. 1952. Twin formation, in cadmium. *Philos. Mag.* 43:422–40

101. Cottrell AH, Bilby BA. 1951. A mechanism for the growth of deformation twins in crystals. *Philos. Mag.* 42:573–81

102. Venables JA. 1961. Deformation twinning in face-centred cubic metals. *Philos. Mag.* 6:379–96

103. Priestner R, Leslie WC. 1965. Nucleation of deformation twins at slip plane intersections in B.C.C. metals. *Philos. Mag.* 11:895–916

104. Sleeswyk AW. 1963. $\frac{1}{2}\langle 111 \rangle$ screw dislocations and the nucleation of $\{112\}\langle 111 \rangle$ twins in the B.C.C. lattice. *Philos. Mag.* 8:1467–86

105. Mahajan S. 1972. Nucleation and growth of deformation twins in Mo-35 at.% Re alloy. *Philos. Mag.* 26:161–71

106. Wasilewski RJ. 1970. Surface distortions in twinned niobium (columbium crystals). *Metall. Trans.* 1:1617–22

107. Vaidya S, Mahajan S. 1980. Accommodation and formation of $\{11\bar{2}1\}$ twins in HCP Co single crystals. *Acta Metall.* 28:1123–31

108. Mahajan S, Chin GY. 1973. Formation of deformation twins in f.c.c. crystals. *Acta Metall.* 21:1353–63

109. Beyerlein IJ, Wang J, Barnett MR, Tomé CN. 2012. Double twinning mechanisms in magnesium alloys via dissociation of lattice dislocations. *Proc. R. Soc. A* 468:1496–520

110. Hirth JP, Lothe J. 1982. *Theory of Dislocations*. Malabar, FL: Krieger. 2nd ed.

111. Xu GS, Argon AS. 2006. Homogeneous nucleation of dislocation loops under stress in perfect crystals. *Philos. Mag. Lett.* 80:605–11

112. Beyerlein IJ, McCabe RJ, Tomé CN. 2011. Effect of microstructure on the nucleation of deformation twins in polycrystalline high-purity magnesium: a multi-scale modeling study. *J. Mech. Phys. Solids* 59:988–1003

113. Kibey S, Liu JB, Johnson DD, Sehitoglu H. 2006. Generalized planar fault energies and twinning in Cu-Al alloys. *Appl. Phys. Lett.* 89:191911

114. Wang J, Beyerlein IJ, Tomé CN. 2014. Reactions of lattice dislocations with grain boundaries in Mg: implications on the micro scale from atomic-scale calculations. *Int. J. Plast.* 56:156–72

115. Beyerlein IJ, Wang J, Kang K, Zheng SJ, Mara NA. 2013. Twinnability of bimetal interfaces in nanostructured composites. *Mater. Res. Lett.* 1:85–89

116. Zheng SJ, Beyerlein IJ, Wang J, Carpenter JS, Han WZ, Mara NA. 2012. Deformation twinning mechanisms from bimetal interfaces as revealed by in situ straining in the TEM. *Acta Mater.* 60:5858–66

117. Mendelson S. 1970. Dislocation dissociations in HCP metals. *J. Appl. Phys.* 41:1893

118. Capolungo L, Beyerlein IJ. 2008. Nucleation and stability of twins in hcp metals. *Phys. Rev. B* 78:024117

119. Vitek V, Kroupa F. 1969. Generalized splitting of dislocations. *Philos. Mag.* 19:265–84

120. Ogata S, Li J, Yip S. 2005. Energy landscape of deformation twinning in bcc and fcc metals. *Phys. Rev. B* 71:224102

121. Van Swygenhoven H, Derlet PM, Frøseth AG. 2004. Stacking fault energies and slip in nanocrystalline metals. *Nat. Mater.* 3:399–403

122. Bernstein N, Tadmor EB. 2004. Tight-binding calculations of stacking energies and twinnability in fcc metals. *Phys. Rev. B* 69:094116

123. Jin ZH, Dunham ST, Gleiter H, Hahn H, Gumbsch P. 2011. A universal scaling of planar fault energy barriers in face-centered cubic metals. *Scr. Mater.* 64:605–8

124. Hunter A, Zhang RF, Beyerlein IJ, Germann TG, Koslowski M. 2013. Dependence of equilibrium stacking fault width in fcc metals on the γ-surface. *Model. Simul. Mater. Sci. Eng.* 21:025015

125. Weertman J. 1961. High velocity dislocations. In *Response of Metals to High Velocity Deformation*, ed. PG Shewmon, VF Zackay, pp. 205–46. New York: Interscience

126. Wang ZQ, Beyerlein IJ. 2008. Stress orientation and relativistic effects on the separation of moving screw dislocations. *Phys. Rev. B* 77:184112

127. Karaman I, Sehitoglu H, Gall K, Chumlyakov YI. 1998. On the deformation mechanisms in single crystal Hadfield manganese steels. *Scr. Mater.* 38:1009–15

128. Zhu YT, Liao XZ, Srinivasan SG, Zhao YH, Baskes MI. 2004. Nucleation and growth of deformation twins in nanocrystalline aluminium. *Appl. Phys. Lett.* 85:5049–51

129. Chen MW, Ma E, Hemker KJ, Sheng HW, Wang YM, Cheng XM. 2003. Deformation twinning in nanocrystalline aluminum. *Science* 300:1275–77

130. Rohatgi A, Vecchio KS, Gray GT III. 2001. A metallographic and quantitative analysis of the influence of stacking fault energy on shock hardening in Cu and Cu–Al alloys. *Acta Mater.* 49:427–38

131. Hughes DA, Lebensohn RA, Wenk HR. 2000. Stacking fault energy and microstructural effects on torsion texture evolution. *Proc. R. Soc. A* 456:921–56

132. Rice JR. 1992. Dislocation nucleation from a crack tip: an analysis based on the Peierls concept. *J. Mech. Phys. Solids* 40:239–71

133. Wang J, Huang H. 2004. Shockley partial dislocations to twin: another formation mechanism and generic driving force. *Appl. Phys. Lett.* 85:5983–85

134. Zhu YT, Wu XL, Liao XZ, Narayan J. 2009. Twinning partial multiplication at grain boundary in nanocrystalline fcc metals. *Appl. Phys. Lett.* 95:031909

135. Wu XL, Liao XZ, Srinivasan SG, Zhou F, Lavernia EJ, et al. 2008. New deformation twinning mechanism generates zero macroscopic strain in nanocrystalline metals. *Phys. Rev. Lett.* 100:095701

136. Li BQ, Li B, Wang YB, Sui ML, Ma E. 2011. Twinning mechanism via synchronized activation of partial dislocations in face-centered-cubic materials. *Scr. Mater.* 64:852–55

137. Pond RC, Serra A, Bacon DJ. 1990. Dislocations in interfaces in the h.c.p. metals—II. Mechanisms of defect mobility under stress. *Acta Mater.* 47:1441–53

138. Zhu YT, Narayan J, Hirth JP, Mahajan S, Wu XL, Liao XZ. 2009. Formation of single and multiple deformation twins in nanocrystalline fcc metals. *Acta Mater.* 57:3763–70

139. Christian JW. 1951. A theory of the transformation in pure cobalt. *Proc. R. Soc. A* 206:51–64

140. Meyers MA, Vohringer O, Lubarda VA. 2001. The onset of twinning in metals: a constitutive description. *Acta Mater.* 49:4025–39

141. Beyerlein IJ, Mara NA, Bhattacharyya D, Necker CT, Alexander DJ. 2011. Texture evolution via combined slip and deformation twinning in rolled silver-copper eutectic nanocomposite. *Int. J. Plast.* 27:121–46

142. Wu XL, Zhu YT, Ma E. 2006. Predictions for partial-dislocation-mediated processes in nanocrystalline Ni by generalized planar fault energy curves: an experimental evaluation. *Appl. Phys. Lett.* 88:121905

143. Rösner H, Markmann J, Weissmuller J. 2004. Deformation twinning in nanocrystalline Pd. *Philos. Mag. Lett.* 84:321–34

144. Liao XZ, Zhou F, Lavernia EJ, He DW, Zhu YT. 2003. Deformation twins in nanocrystalline Al. *Appl. Phys. Lett.* 83:5062–64

145. Yamakov V, Wolf D, Phillpot SR, Mukherjee AK, Gleiter H. 2004. Deformation-mechanism map for nanocrystalline metals by molecular-dynamics simulation. *Nat. Mater.* 3:43–47139

146. Asaro RJ, Krysl P, Kad B. 2003. Deformation mechanism transitions in nanoscale fcc metals. *Philos. Mag. Lett.* 83:733–43

147. Zhu YT, Liao XZ, Srinivasan SG, Lavernia EJ. 2005. Nucleation of deformation twins in nanocrystalline face-centered-cubic metals processed by severe plastic deformation. *J. Appl. Phys.* 98:034319

148. Hunter A, Beyerlein IJ. 2014. Stacking fault emission from grain boundaries: material dependencies and grain size effects. *Mater. Sci. Eng. A* 600:200–10

149. Hunter A, Beyerlein IJ. 2013. Unprecedented grain size effect on stacking fault width. *Appl. Phys. Lett. Mater.* 1:032109

150. Zhang RF, Beyerlein IJ, Germann TC, Wang J. 2011. Deformation twinning in bcc metals under shock loading: a challenge to empirical potentials. *Philos. Mag. Lett.* 91:731–40

151. Schoeck G. 1966. Nucleation of deformation twins in F.C.C. metals. *Phys. Status Solidi* 13:K127–30

152. Marian J, Cai W, Bulatov VV. 2004. Dynamic transitions from smooth to rough to twinning in dislocation motion. *Nat. Mater.* 3:158–63

153. Ogawa K. 1965. Edge dislocations dissociated in {112} planes and twinning mechanism of B.C.C. metals. *Philos. Mag.* 11:217–33

154. Chu HJ, Wang J, Beyerlein IJ. 2012. Anomalous reactions of a supersonic coplanar dislocation dipole: bypass or twinning? *Scr. Mater.* 67:69–72

155. Kronberg ML. 1961. Atom movements and dislocation structures in some common crystals. *Acta Metall.* 9:970–72

156. Barnett MR, Keshavarz Z, Beer AB, Ma X. 2008. Non-Schmid behavior during secondary twinning in a polycrystalline magnesium alloy. *Acta Mater.* 56:5–15

157. Mu S, Jonas JJ, Gottstein G. 2012. Variant selection of primary, secondary, and tertiary twins in a deformed Mg alloy. *Acta Mater.* 60:2043–53

158. Proust G, Kaschner GC, Beyerlein IJ, Clausen B, Brown DW, et al. 2010. Detwinning of high-purity zirconium: in-situ neutron diffraction experiments. *Exp. Mech.* 50:125–33

159. Pond RC, Hirth JP. 1994. Defects at surfaces and interfaces. *Solid State Phys.* 47:287–365

160. Wang J, Beyerlein IJ, Hirth JP. 2012. Nucleation of elementary $\{\bar{1}011\}$ and $\{\bar{1}013\}$ twinning dislocations at a twin boundary in hexagonal close-packed crystals. *Model. Simul. Mater. Sci. Eng.* 20:024001

161. Serra A, Pond RC, Bacon DJ. 1991. Computer simulation of the structure and mobility of twinning dislocations in H.C.P. metals. *Acta Metall. Mater.* 39:1469–80

162. Serra A, Bacon DJ. 1996. A new model for $\{10\bar{1}2\}$ twin growth in HCP metals. *Philos. Mag.* 73:333–43

163. Wang J, Hoagland RG, Hirth JP, Capolungo L, Beyerlein IJ, Tomé CN. 2009. Nucleation of a $(\bar{1}012)$ twin in hexagonal-close-packed crystals. *Scr. Mater.* 61:903–6

164. Le Lann A, Dubertret A. 1979. A development of Kronberg's model for $\{1012\}$ twins in H.C.P. metals. Extension to $\{1122\}$ twins. *Phys. Status Solidi* 51:497–507

165. Dubertret A, Le Lann A. 1980. Development of a new model for atom movement in twinning. Case of the $\{1011\}$, $\{1013\}$ twins and $\{1011\}$ $\{1012\}$ double twinning in H.C.P. metals. *Phys. Status Solidi* 60:145–51

166. Song SG, Gray GT III. 1995. Structural interpretation of the nucleation and growth of deformation twins in Zr and Ti—1. Application of the coincidence site lattice (CSL) theory to twinning problems in h.c.p. structures. *Acta Metall. Mater.* 43:2325–37

167. Li B, Ma E. 2009. Atomic shuffling dominated mechanism for deformation twinning in magnesium. *Phys. Rev. Lett.* 103:035503

168. Xu B, Capolungo L, Rodney D. 2013. On the importance of prismatic/basal interfaces in the growth of $(\bar{1}012)$ twins in hexagonal close-packed crystals. *Scr. Mater.* 68:901–4

169. Yu Q, Qi L, Mishra RK, Minor AM. 2013. Reducing deformation anisotropy to achieve ultrahigh strength and ductility in Mg at the nanoscale. *Proc. Nat. Acad. Sci. USA* 110:13289–93

170. Tsai MS, Chang CP. 2013. Grain size effect on deformation twinning in Mg–Al–Zn alloy. *Mater. Sci. Tech.* 29:759–63

171. Han J, Su XM, Jim ZH, Zhu YT. 2011. Basal-plane stacking-fault energies of Mg: a first-principles study of Li- and Al-alloying effects. *Scr. Mater.* 64:693–96

172. Li B, Ma E. 2009. Zonal dislocations mediating $\{10\bar{1}1\}\langle 10\bar{1}\bar{2}\rangle$ twinning in magnesium. *Acta Mater.* 57:1734–43

173. Carpenter JS, McCabe RJ, Zheng SJ, Wynn TA, Mara NA, Beyerlein IJ. 2014. Processing parameter influence on texture and microstructural evolution in Cu-Nb multilayer composites fabricated via accumulative roll bonding. *Metall. Mater. Trans. A* 45:2192–208

174. Carpenter JS, Zheng SJ, Zhang RF, Vogel SC, Beyerlein IJ, Mara NA. 2013. Thermal stability of Cu–Nb nanolamellar composites fabricated via accumulative roll bonding. *Philos. Mag.* 93:718–35

175. Beyerlein IJ, Caro A, Demkowicz MJ, Mara NA, Misra A, Uberuaga BP. 2013. Radiation damage tolerant nanomaterials. *Mater. Today.* 16:443–49

176. Monclús MA, Zheng SJ, Mayeur JR, Beyerlein IJ, Mara NA, et al. 2013. Optimum high temperature strength of two-dimensional nanocomposites. *Appl. Phys. Lett. Mater.* 1:052103

177. Han WZ, Cerreta EK, Mara NA, Beyerlein IJ, Misra A. 2013. Deformation and failure of shocked bulk Cu–Nb nanolaminates. *Acta Mater.* 63:150–61

178. Han WZ, Demkowicz MJ, Mara NA, Fu E, Sinha S, et al. 2013. Design of radiation tolerant materials via interface engineering. *Adv. Mater.* 25:6975–79

179. Lee KH, Hong SI. 2003. Interfacial and twin boundary structures of nanostructured Cu–Ag filamentary composites. *J. Mater. Res.* 18:2194–202

180. Han K, Hirth JP, Embury JD. 2001. Modeling the formation of twins and stacking faults in the Ag–Cu system. *Acta Mater.* 49:1537–40

181. Han K, Lawson AC, Wood JT, Embury JD, Von Dreele RB, Richardson JW Jr. 2004. Internal stresses in cold-deformed Cu–Ag and Cu–Nb wires. *Philos. Mag.* 84:2579–93

182. Wang J, Beyerlein IJ, Mara NA, Bhattacharyya D. 2011. Interface-facilitated deformation twinning in copper within submicron Ag-Cu multilayered composites. *Scr. Mater.* 64:1083–86

183. Misra A, Hirth JP, Hoagland RG, Embury JD, Kung H. 2004. Dislocation mechanisms and symmetric slip in rolled nano-scale metallic multilayers. *Acta Mater.* 52:2387–94

184. Lee SB, LeDonne JE, Lim SCV, Beyerlein IJ, Rollett AD. 2012. The five-parameter heterophase interface character distribution (HICD) of physical vapor-deposited and accumulative roll-bonded Cu-Nb multilayer composites. *Acta Mater.* 60:1747–61

185. Carpenter JS, McCabe RJ, Beyerlein IJ, Wynn TA, Mara NA. 2013. A wedge-mounting technique for nanoscale electron backscatter diffraction. *J. Appl. Phys.* 113:094304

186. Zheng SJ, Beyerlein IJ, Carpenter JS, Kang K, Wang J, et al. 2013. High strength and thermal stability due to twin-induced interfaces. *Nat. Commun.* 4:1696

187. Beyerlein IJ, Wang J, Zhang RF. 2013. Mapping dislocation nucleation behavior from bimetal interfaces. *Acta Mater.* 61:7488–99

188. Beyerlein IJ, Mara NA, Wang J, Carpenter JS, Zheng SJ, et al. 2012. Structure-property-functionality of bimetal interfaces. *JOM* 64(10):1192–207

Contents

Index

Errata

An online log of corrections to *Annual Review of Materials Research* articles may be
found at http://www.annualreviews.org/errata/matsci

ANNUAL REVIEWS

It's about time. Your time. It's time well spent.

New From Annual Reviews:

Annual Review of Statistics and Its Application

Volume 1 • Online January 2014 • http://statistics.annualreviews.org

Editor: **Stephen E. Fienberg,** *Carnegie Mellon University*

Associate Editors: **Nancy Reid,** *University of Toronto*

Stephen M. Stigler, *University of Chicago*

The *Annual Review of Statistics and Its Application* aims to inform statisticians and quantitative methodologists, as well as all scientists and users of statistics about major methodological advances and the computational tools that allow for their implementation. It will include developments in the field of statistics, including theoretical statistical underpinnings of new methodology, as well as developments in specific application domains such as biostatistics and bioinformatics, economics, machine learning, psychology, sociology, and aspects of the physical sciences.

Complimentary online access to the first volume will be available until January 2015.

Access this and all other Annual Reviews journals via your institution at www.annualreviews.org.

ANNUAL REVIEWS | Connect With Our Experts

Tel: 800.523.8635 (US/CAN) | Tel: 650.493.4400 | Fax: 650.424.0910 | Email: service@annualreviews.org